

# JGR Atmospheres

## RESEARCH ARTICLE

10.1029/2020JD034108

### Key Points:

- We evaluate the separate and combined biophysical vegetation effects on hydroclimate in a high-CO<sub>2</sub> world using the GISS ModelE global climate model
- Increased leaf areas enhance soil moisture drying at lower latitudes; reduced stomatal conductance enhances high-latitude warming
- Increased leaf area and reduced stomatal conductance also produce complex nonlinear and either competing or mutually amplifying regional hydroclimate responses

### Supporting Information:

- Supporting Information S1

### Correspondence to:

S. S. McDermid,  
[sps246@nyu.edu](mailto:sps246@nyu.edu)

### Citation:

McDermid, S. S., Cook, B. I., De Kauwe, M. G., Mankin, J., Smerdon, J. E., Williams, A. P., et al. (2021). Disentangling the regional climate impacts of competing vegetation responses to elevated atmospheric CO<sub>2</sub>. *Journal of Geophysical Research: Atmospheres*, 126, e2020JD034108. <https://doi.org/10.1029/2020JD034108>

Received 16 OCT 2020

Accepted 24 JAN 2021

© 2021. The Authors.

This is an open access article under the terms of the [Creative Commons Attribution-NonCommercial License](https://creativecommons.org/licenses/by-nc/4.0/), which permits use, distribution and reproduction in any medium, provided the original work is properly cited and is not used for commercial purposes.

## Disentangling the Regional Climate Impacts of Competing Vegetation Responses to Elevated Atmospheric CO<sub>2</sub>

Sonali Shukla McDermid<sup>1,2</sup> , Benjamin I. Cook<sup>2,3</sup> , Martin G. De Kauwe<sup>4,5,6</sup>, Justin Mankin<sup>3,7</sup> , Jason E. Smerdon<sup>3</sup> , A. Park Williams<sup>3</sup> , Richard Seager<sup>3</sup> , Michael J. Puma<sup>2,8</sup>, Igor Aleinov<sup>2,8</sup> , Maxwell Kelley<sup>2</sup>, and Larissa Nazarenko<sup>2,8</sup> 

<sup>1</sup>Department of Environmental Studies, New York University, New York, NY, USA, <sup>2</sup>NASA Goddard Institute for Space Studies, New York, NY, USA, <sup>3</sup>Lamont-Doherty Earth Observatory of Columbia University, Palisades, NY, USA, <sup>4</sup>ARC Centre of Excellence for Climate Extremes, Sydney, NSW, Australia, <sup>5</sup>Change Research Centre, University of New South Wales, Sydney, NSW, Australia, <sup>6</sup>Evolution & Ecology Research Centre, University of New South Wales, Sydney, NSW, Australia, <sup>7</sup>Department of Geography, Dartmouth College, Hanover, NH, USA, <sup>8</sup>Center for Climate Systems Research, Columbia University, New York, NY, USA

**Abstract** Biophysical vegetation responses to elevated atmospheric carbon dioxide (CO<sub>2</sub>) affect regional hydroclimate through two competing mechanisms. Higher CO<sub>2</sub> increases leaf area (LAI), thereby increasing transpiration and water losses. Simultaneously, elevated CO<sub>2</sub> reduces stomatal conductance and transpiration, thereby increasing rootzone soil moisture. Which mechanism dominates in the future is highly uncertain, partly because these two processes are difficult to explicitly separate within dynamic vegetation models. We address this challenge by using the GISS ModelE global climate model to conduct a novel set of idealized 2×CO<sub>2</sub> sensitivity experiments to: evaluate the total vegetation biophysical contribution to regional climate change under high CO<sub>2</sub>; and quantify the separate contributions of enhanced LAI and reduced stomatal conductance to regional hydroclimate responses. We find that increased LAI exacerbates soil moisture deficits across the sub-tropics and more water-limited regions, but also attenuates warming by ~0.5–1°C in the US Southwest, Central Asia, Southeast Asia, and northern South America. Reduced stomatal conductance effects contribute ~1°C of summertime warming. For some regions, enhanced LAI and reduced stomatal conductance produce nonlinear and either competing or mutually amplifying hydroclimate responses. In northeastern Australia, these effects combine to exacerbate radiation-forced warming and contribute to year-round water limitation. Conversely, at higher latitudes these combined effects result in less warming than would otherwise be predicted due to nonlinear responses. These results highlight substantial regional variation in CO<sub>2</sub>-driven vegetation responses and the importance of improving model representations of these processes to better quantify regional hydroclimate impacts.

## 1. Introduction

The increasing atmospheric concentration of carbon dioxide (CO<sub>2</sub>) can impact global ecosystems through its effects on climate and also through its direct effects on plants. In fact, enhanced CO<sub>2</sub> has likely played an important role in historical trends of global ecosystem change (Donohue et al., 2013; Myneni et al., 1997; Walker et al., 2020; Zhu et al., 2016), although the magnitude of these CO<sub>2</sub> effects relative to other drivers (e.g., human land management) varies regionally (Chen et al., 2019; Donohue et al., 2013; Forkel et al., 2016; Van Der Sleen et al., 2015). Increasing CO<sub>2</sub> can enhance primary productivity and biospheric carbon uptake, provided other conditions (e.g., nutrients and water) are not limiting (Arneeth et al., 2010; Norby et al., 2005; Reich et al., 2014). The full biophysical response of vegetation nevertheless consists of multiple, sometimes competing, physiological interactions that are still poorly constrained, especially at regional scales (Chen et al., 2019; Fatichi et al., 2016; Forzieri et al., 2017; Mankin et al., 2017; Norby & Zak, 2011). These interactions can, in turn, significantly influence regional climate and hydrology, particularly through two key physiological mechanisms. First, elevated CO<sub>2</sub> is expected to reduce stomatal conductance, increase plant water use efficiency and ameliorate evaporative losses of water from the surface (Eamus & Jarvis, 1989; Morgan et al., 2011; Morison, 1985; Sellers et al., 1996; Swann et al., 2016). Second, higher CO<sub>2</sub> is also expected to

increase leaf area (Norby & Zak, 2011) and the effective evaporative area at the surface, which can increase total ecosystem-level evapotranspiration (ET) (Lemordant et al., 2018; Mankin et al., 2017, 2018, 2019). The aggregate water cycle response to climate change at the surface may therefore depend on the balance of these two highly uncertain processes (Norby & Zak, 2011) and whether one is likely to dominate over the other in a warmer, higher CO<sub>2</sub> world.

Reduced stomatal conductance, resulting in attenuated transpiration and latent heat fluxes, can amplify surface warming (in a feedback known as physiological forcing), but can also ameliorate soil moisture losses (Andrews et al., 2011; Douville et al., 2000; Kala et al., 2015, 2016; Kergoat et al., 2002; Kovenock & Swann, 2018; Skinner et al., 2018). This increase in warming is most prominent during summer over highly vegetated areas in the northern mid-latitudes (Kergoat et al., 2002; Kovenock & Swann, 2018) and over tropical forests (Andrews et al., 2011; Douville et al., 2000; Pu & Dickinson, 2014). Reduced stomatal conductance may also force reductions in global precipitation rates by suppressing convective activity and increasing the likelihood of dry day occurrences (Andrews et al., 2011; Skinner et al., 2017). Along coastal areas and in tropical forests (e.g., the inland Amazon), enhanced warming from reduced conductance may drive regionalized atmospheric circulation changes and subsequent atmospheric moisture convergence (Chadwick et al., 2019; Pu & Dickinson, 2014; Saint-Lu et al., 2019; Skinner et al., 2017). Douville et al. (2000) suggest that such circulation changes may also drive counterintuitive responses in regions of tighter land-atmosphere coupling, such as a cooling over the Indian peninsula and a cooling/warming dipole-like response across Europe.

In contrast, higher leaf area can also enhance growing-season ET, particularly in relatively wet environments (Betts et al., 1997; Forzieri et al., 2017; Lemordant et al., 2018; Mankin et al., 2017), although the strength of this effect may diminish at lower latitudes (Betts et al., 1997; Pu & Dickinson, 2014) and at higher levels of CO<sub>2</sub> (Skinner et al., 2018). There is increasing interest to identify and classify global ET trends. For example, Jung et al. (2010) used a machine learning algorithm to estimate global ET by integrating point-based FLUXNET ET, vegetation information, meteorological measurements, and satellite estimates of fraction of photosynthetically active radiation absorbed by the canopy. They found an increasing trend until the late 20th century after which point the growth rate plateaued (Jung et al., 2010). In a more recent analysis, Zhang et al. (2015) applied a process-based land surface algorithm to estimate global terrestrial ET and PET using satellite estimates of photosynthetic canopy cover and meteorological inputs and showed that the global positive ET trend extended to 2013. However, these globally-averaged trends may belie important regional variation in vegetation water responses (Mankin et al., 2019). For example, in Northern Hemisphere mid-to-high latitude forests, increasing water use efficiency may be driving reductions in ET (Keenan et al., 2013). In contrast, both humid and arid Australian river basins have not displayed strong or significant ET responses (Ukkola et al., 2016). Outside of these areas, however, increasing ET trends may induce soil moisture losses, reduced runoff, and exacerbate regional drying despite enhanced stomatal regulation (Douville et al., 2000; Frank et al., 2015; Kergoat et al., 2002; Swann, 2018). Such responses may be particularly important in arid and semi-arid environments like the American Southwest and sub-humid to semi-arid river basins in Australia (Fatichi et al., 2016; Mankin et al., 2017; Trancoso et al., 2017; Ukkola et al., 2016). At the same time, enhanced latent heat fluxes resulting from higher leaf areas can reduce regional warming in semi-arid and subtropical regions (Forzieri et al., 2017; Zeng et al., 2017).

The resulting hydrological response of these combined effects are variable and highly dependent on regional background climate conditions (Forzieri et al., 2017; Mankin et al., 2019; Swann, 2018; Swann et al., 2016). While some studies (described above) suggest that enhanced leaf area may cancel the water savings from reduced stomatal conductance, others highlight that many non-forested areas have environmental limitations on leaf area growth (e.g. water, radiation, photosynthetic pathway) (Betts et al., 1997; Bounoua et al., 2010; Pu & Dickinson, 2014), or that plants will acclimate their leaf structure to higher CO<sub>2</sub> (Poorter et al., 2019), thereby geographically constraining their climate effects. Skinner et al. (2018) suggest that only regions with the largest proportional leaf area increases would compensate for the generally stronger and more pervasive effects of reduced conductance. As such, the combined stomatal conductance and leaf area responses in model simulations display an overall tendency toward reduced transpiration across most vegetated areas (Chadwick et al., 2019; Pu & Dickinson, 2014; Skinner et al., 2018) and an increase in plant water use efficiency. However, if plant biomass increases due to CO<sub>2</sub> fertilization, increased water use

efficiency would not necessarily translate to reductions in total plant water demand (Mooney et al., 1991; Skinner et al., 2018). Furthermore, there are a host of other plant physiological responses to CO<sub>2</sub> that can modulate both conductance and leaf area, including photosynthetic downregulation (Bounoua et al., 2010; Kovenock & Swann, 2018; Pu & Dickinson, 2014) and leaf trait acclimation, such as increasing leaf thickness (Kovenock & Swann, 2018; Swann, 2018), that may further reduce overall global ET, but these effects are still not well-constrained (Swann, 2018).

Most previous work to disentangle these varied effects of increased CO<sub>2</sub> used dynamic global vegetation models (DGVMs) but these models do not fully represent all the above-described CO<sub>2</sub>-vegetation-climate interactions, processes, and/or reproduce observed responses (Fatichi et al., 2016; Smith et al., 2015; Swann, 2018). For example, when compared with FACE experiments DGVMs can qualitatively produce initial net primary production (NPP) increases with rising CO<sub>2</sub>, but representations of key plant processes (e.g. nitrogen uptake) and, consequently, their overall longer-term responses still exhibit substantial error (Medlyn et al., 2015). In comparison to satellite-based NPP estimates, DGVMs in current Earth System Models may be overly sensitive to CO<sub>2</sub>-fertilization effects (Smith et al., 2015). On the other hand, these satellite-based estimates may themselves be prone to under-prediction and one must be cautious when conducting model-data comparisons – identifying appropriate metrics and site-based comparisons remain critical for model evaluation (De Kauwe et al., 2016). Even more fundamentally, there still exists structural uncertainty about carbon allocation to various plant structures under higher CO<sub>2</sub>, which complicates future projections of hydroclimate change (De Kauwe et al., 2014; J. Yang et al., 2018). As a consequence, DGVMs may underestimate the effects of regional drying and soil moisture losses resulting from plant physiological feedbacks (Smith et al., 2015). The few studies that undertook much-needed model sensitivity tests either do not explicitly isolate leaf area from conductance effects (e.g., Bounoua et al., 2010; Pu & Dickinson, 2014) or include regional constraints on leaf area growth that may inhibit a deeper probing and understanding of vegetation sensitivities to higher CO<sub>2</sub> (Pu & Dickinson, 2014). Finally, there are a host of other limitations to plant growth, including nutrient cycling (Wieder et al., 2015; Zaehle et al., 2014), pest/diseases, fire, and climate extremes that may obscure CO<sub>2</sub> effects, driving further inconsistencies between models and observations (Reich et al., 2014).

While it remains challenging to comprehensively simulate dynamic vegetation responses to elevated CO<sub>2</sub>, more controlled climate model experiments provide opportunities to isolate these biophysical vegetation effects and assess their relative and additive contributions to modeled regional hydroclimate changes. We therefore design a novel set of global climate model (GCM) sensitivity experiments: first using an idealized approach implementing large, uniform (50%) leaf area increases and second constraining LAI increases using a multi-model ensemble from the Sixth Coupled Model Intercomparison Project (CMIP6, Eyring et al., 2016). Furthermore, most of the above-described studies have evaluated either vegetation biophysical responses in the absence of enhanced radiative forcing or their combined interaction (i.e., reduced stomatal conductance and CO<sub>2</sub> fertilization) under high CO<sub>2</sub>. In contrast, our experiments are novel for they are among the few to explicitly evaluate both the competing and combined influences of reduced stomatal conductance and enhanced LAI all in an elevated CO<sub>2</sub> world. We use this experimental design to answer the following research questions in a modeling context: (i) What are the separate effects of CO<sub>2</sub>-induced radiative warming, reduced stomatal conductance, and enhanced leaf area on the global and regional hydroclimate?; (ii) How do these effects combine to create the full CO<sub>2</sub>-vegetation biophysical response?; and (iii) How do these effects interact (e.g., amplify, diminish, or dominate each other) regionally?

## 2. Methods

### 2.1. Experimental Design

We perform our experiments with the NASA GISS ModelE, a state-of-the-art global climate model that contributes to the Coupled Model Intercomparison Project (CMIP, Eyring et al., 2015) as an ongoing development effort. The most recent documented version is described in Miller et al. (2014), Schmidt et al. (2014), and Kelley et al. (2020). ModelE runs at 2° × 2.5° spatial resolution with 40 vertical layers in the atmosphere and has been shown to reasonably represent observed climate conditions and responses to historical anthropogenic forcings (Miller, 2014; Schmidt et al., 2014). For this study, we use a q-flux ocean configured to reproduce a pre-industrial SST climatology (1876–1885) (Schmidt et al., 2006). This allows the sea surface to

**Table 1**  
*Individual experiment design*

Experiment	Effects enabled
Baseline	Pre-industrial radiative forcings; natural vegetation with nominal LAI and conductance effects “on”
CO2_only	2×CO <sub>2</sub> ; natural vegetation with default LAI and conductance effects “off”
CO2+Con	2×CO <sub>2</sub> ; natural vegetation with default LAI and conductance effects “on”
CO2+LAI <sub>50</sub>	2×CO <sub>2</sub> ; natural vegetation with enhanced 50% LAI and conductance effects “off”
CO2+LAI <sub>50</sub> +Con	2×CO <sub>2</sub> ; natural vegetation with enhanced 50% LAI and conductance effects “on”
CO2+LAI <sub>CMIP</sub>	2×CO <sub>2</sub> ; natural vegetation with “pseudo” 2×CO <sub>2</sub> LAI and conductance effects “off”
CO2+LAI <sub>CMIP</sub> + Con	2×CO <sub>2</sub> ; natural vegetation with “pseudo” 2×CO <sub>2</sub> LAI and conductance effects “on”

interact with the overlying atmosphere via surface heat fluxes and generate SST anomalies while the ocean heat flux convergence due to currents is prescribed and held fixed. For each experiment, the model was run with initial conditions taken from a randomly selected year of a previously-equilibrated q-flux experiment, based on the same SST interval and with no additional forcings (~1850 conditions).

We conduct seven experiments (detailed in Table 1) with various combinations of stomatal conductance and LAI effects enabled to disentangle the impact of each response on regional climate. The last 50 years of 101-years integration periods are used for our analyses. The 2×CO<sub>2</sub> radiative forcing is set to 560 ppm at the beginning of the simulation, while all other forcings remain at pre-industrial levels. In experiments where the conductance effects are turned “off,” the vegetation sees pre-industrial CO<sub>2</sub> concentrations (280 ppm) within the model framework and thus conductance does not respond to the elevated atmospheric CO<sub>2</sub>. Two of the experiments are forced with prescribed LAI increases, in which we artificially increase the default monthly LAIs for each vegetation type by 50% (Figure 1a).

This large increase is intended to test the sensitivity of the overall vegetation responses and is not intended to reflect the response of individual vegetation types to higher CO<sub>2</sub>, as these vary widely and are subject to large uncertainties (Swann, 2018). Similar modeling studies using prescribed LAI constrained by environmental limitations show LAI increases of ~30% (Pu & Dickinson, 2014). Site-based LAI response curves from Free-Air Carbon Enrichment (FACE) experiments indicate that the maximum LAI change in a few of the vegetation types assessed could be greater than 30% but are generally less than 50%, and that plant types with relatively small initial LAI values increased the most (Norby & Zak, 2011). We further note that in DGVMs, there exists a large range of predicted mean global LAI under current conditions and several models produce LAIs nearly twice that of satellite-based estimates (Mahowald et al., 2016).

Nevertheless, to better contextualize these hydroclimate responses, we further augment these sensitivity tests with two additional experiments in which the prescribed LAI forcing is constrained by the newest contributions to CMIP6. Our intent is to separate the high CO<sub>2</sub> radiative forcing and the plant physiological responses, and, thus, we choose a high CO<sub>2</sub> experiment with the greatest number of models reporting LAI. At the time of this writing, there are a limited number of models that have submitted simulations and/or are reporting LAI for the abrupt 2×CO<sub>2</sub> experiment, which prohibits a reasonable multi-model ensemble for comparison. As such, we instead use LAI results produced by nine models from the abrupt 4×CO<sub>2</sub> experiment and compute a simplified “pseudo” 2×CO<sub>2</sub> response with the following approach: (1) for each of the nine models, we first compute monthly LAI climatologies for both the abrupt 4×CO<sub>2</sub> and pre-industrial simulations using the last 30 years of each experiment. (2) We then take the monthly, spatially explicit, significant differences (per a Student’s t-test) between these experiments and add *half* these differences to the pre-industrial LAI. This constitutes our “pseudo” 2×CO<sub>2</sub> experiment as we assume linearity of the LAI response to increasing CO<sub>2</sub>. (3) We then regrid each model’s native resolution to ModelE resolution using a bilinear approach, compute the ensemble average for both the pre-industrial and “pseudo” 2×CO<sub>2</sub> experiments, and take the percent change from our “pseudo” 2×CO<sub>2</sub> experiment relative to the pre-industrial.

The resulting LAI change for this “pseudo” 2×CO<sub>2</sub> experimental response is shown in Figure 1c. Spatial patterns and magnitudes of LAI change are broadly consistent with our prescribed 50% LAI increases. The

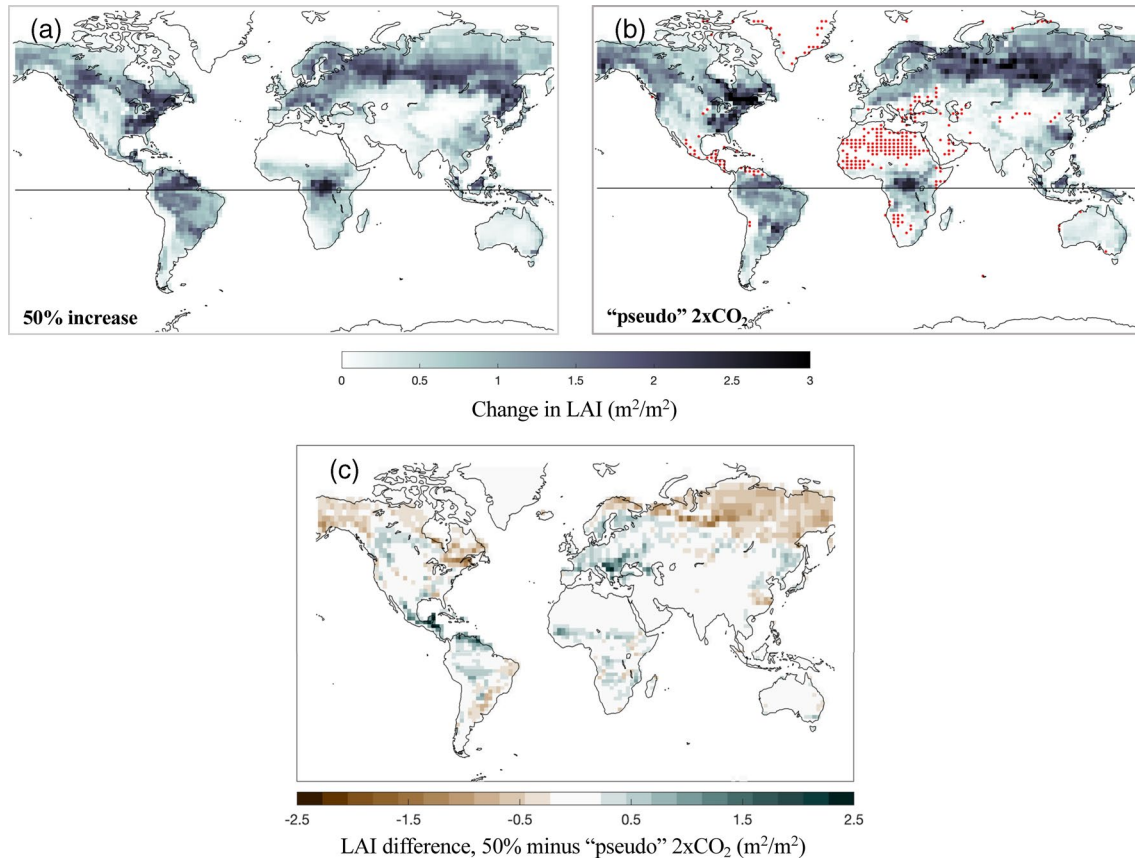


**Figure 1.** The change in peak growing season LAI (aggregated across vegetation types) from Baseline for (a) 50% increase sensitivity experiment and (b) CMIP6 “pseudo”  $2\times\text{CO}_2$  ensemble. Red markers indicate small LAI decreases. Both panels (a) and (b) use colorbar under (b). (c) Fractional (0–1) coverage per gridcell of C4 grass used in modelE. (d) Difference in peak growing season LAI for 50% increase sensitivity experiment minus CMIP6 “pseudo”  $2\times\text{CO}_2$  experiment.

global, annually averaged increase in this “pseudo”  $2\times\text{CO}_2$  multi-model ensemble was  $\sim 50\%$  (49.6%) relative to pre-industrial LAI, but this value embeds significant regional heterogeneity in the CMIP6 models’ simulated LAI changes. Some low latitude areas, which are sparsely vegetated, and/or significantly comprised of  $\text{C}_4$  vegetation, show slight reductions in LAI (red dots in Figure SI9), with a maximum decline of approximate  $-0.4 \text{ m}^2/\text{m}^2$ . Such declines, although small, are not accounted for in the design of our 50% LAI increase experiment. Additionally, most models displayed LAI increases upwards of several hundred percent under abrupt  $4\times\text{CO}_2$  conditions in sparsely vegetated areas or areas of relatively low canopy density. We limited the inclusion of extremely high LAI percent changes by capping the percent change at 100, which will attenuate some regional and the global percent change reported above. We also imposed no LAI changes where vegetation did not exist in the preindustrial experiment, but was included in the  $4\times\text{CO}_2$  (e.g. due to model determination of suitable climate conditions). The spatial heterogeneity in regional LAI responses is more evident when compared directly to our 50% LAI increase (Figure 1c). The latter generally shows higher LAI values in the tropics, where the CMIP6 “pseudo”  $2\times\text{CO}_2$  does not display as strong a sensitivity, and lower LAIs at higher latitudes, particularly in the Northern Hemisphere. Results and comparisons for this “pseudo”  $2\times\text{CO}_2$  experiment are presented in Section 3.6.

## 2.2. Configuration of ModelE’s Land Surface and Vegetation

ModelE uses vegetation characteristics from the Ent Terrestrial Biosphere Model (Ent TBM), which was developed around the height structured cohorts and subgrid patch communities of the Ecosystem Demography model (Medvigy et al., 2009; Moorcroft et al., 2001). The Ent canopy radiative transfer uses the Analytical Clumped TwoStream (ACTS) scheme to calculate the clumping of foliage in mixed, vertically layered canopies (NiMeister et al., 2010; Yang et al., 2010). Ent biophysics are based on well-known coupled

photosynthesis and stomatal conductance formulation (Ball et al., 1987; Collatz et al., 1992; Farquhar & von Caemmerer, 1982). For our experiments, we operate Ent in “biophysics-only” mode as described by Kim et al. (2015). In this mode, water vapor fluxes are prognostically simulated for each grid cell by prescribing canopy structure and maximum and minimum leaf area index (LAI) for 17 possible Plant Functional Types (PFTs). Further details about the natural vegetation phenology and the canopy radiative transfer can be found in Kim et al. (2015) and Friend and Kiang (2005), respectively.

We used prescribed natural vegetation distributions from the MODIS (MCD12Q1 V005 L3) International Geosphere-Biosphere Program (IGBP) land cover product at  $0.5^\circ \times 0.5^\circ$  latitude  $\times$  longitude. MODIS PFTs for the year 2004 (Friedl et al., 2010) were classified into sub-grid cover fractions most closely matching the Ent PFTs using additional data on forest heights (Simard et al., 2011) and climate (Harris et al., 2014; Schneider et al., 2014). To represent vegetation phenology, monthly prescribed values from the MODIS (MOD15A2 V004, L4) LAI product (Tian et al., 2002a, 2002b; W. Yang et al., 2006) were matched to the above-described sub-grid Ent PFT fractions. This distribution was then aggregated to the ModelE grid resolution of  $2^\circ \times 2.5^\circ$  latitude  $\times$  longitude. Aggregating the MODIS natural vegetation types for use with Ent PFTs at the ModelE resolution does attenuate the extreme regional values, as many cells have either relatively low LAIs or higher LAIs with relatively low areal coverage. Within the model simulations, the monthly prescribed LAIs are linearly interpolated to create a daily time series. Currently, snow-free surface albedo does not depend on LAI in the Ent biophysics-only mode of operation and these effects are, thus, excluded from our analysis. We do, however, acknowledge the importance of such albedo effects in radiation-vegetation interactions and discuss their potential implications in Section 3.7.

Latent heat fluxes from the surface are separated between the vegetated and non-vegetated portions of each grid cell. For vegetated grid cell fractions, the evapotranspiration term is the sum of four components: transpiration, canopy evaporation from leaf surfaces, soil evaporation, and snow sublimation. Transpiration follows an aerodynamic formulation specified in Hansen et al. (1983) and Rosenzweig and Abramopoulos (1997), which is dependent on canopy conductance, atmospheric conductance, and the saturated and unsaturated air humidity. For soil evaporation under the canopy, a modification is made to the turbulent transfer coefficient to account for wind/leaf interactions. For the bare soil fraction of the grid cell, evaporation occurs as the minimum of the Penman potential evaporation or Gardner-Hillel diffusivity (Abramopoulos et al., 1988). Canopy evaporation is assumed to occur at the potential rate.

The land surface and vegetation characteristics can also impact the atmospheric planetary boundary layer (PBL), which in turn can influence and even lead to preferential precipitation over dry soils (C. M. Taylor et al., 2012). ModelE’s PBL uses a formulation for the temperature, moisture, and scalar fluxes, comprised of diffusive and counter-gradient terms based on large-eddy simulation data of Holtslag and Moeng (1991). Following Holtslag and Moeng (1991), the counter-gradient term is scaled by the surface flux of each quantity, and that flux is effectively distributed over the PBL per a parameterized profile that depends on the PBL height (Schmidt et al., 2006). The second-order closure model by Cheng et al. (2002) is used above the PBL, and a few turbulent time scales are given by the two-point turbulence closure model of Canuto and Dubovikov (1996). The length scale is given by Holtslag and Boville (1993). Additional details, the resulting improvements in PBL simulation, and comparisons with observations are reported in Schmidt et al. (2006; 2014).

### 2.3. Experiment Evaluation

In order to evaluate the isolated effects of  $2\times\text{CO}_2$ , reduced conductance, and enhanced LAI—and consider their combined interactions—we calculated anomalies between our respective experiments, described in Table 2. These anomalies (named in Column 1 of Table 2) will serve as our basis for evaluation throughout the Results section. We focus most of our analysis on regional hydroclimate impacts, using more “plant-centric” variables (Swann et al., 2016), for example soil moisture and evaporative fraction, in order to better bracket the ecological implications for future drought dynamics. Soil moisture anomalies between experiments are shown as a “z-score,” divided by the standard deviation of the reference experiment (Table 2) and taken for the top 57 cm. To better understand soil moisture sensitivity to these plant physiological effects, we additionally provide soil moisture changes at approximately 1- and 2-m depths for BioPhys, Con\_Only, and LAI\_only (SI Figure 3). Furthermore, the climate anomalies shown include nonlinear interactions that

**Table 2**  
*The isolated forcing responses*

Effect name	Anomaly taken	Description of effect/eesponse
Rad_Only	CO2_only <i>minus</i> Baseline	Isolates the climate response to the change in radiative forcing only, excluding the direct vegetation biophysical effects
Con_Only	CO2+LAI <sub>50</sub> +Con <i>minus</i> CO2+LAI <sub>50</sub>	Isolates the climate response to reduced stomatal conductance, excluding the direct radiative and enhanced 50% LAI effects
LAI_Only	CO2+LAI <sub>50</sub> +Con <i>minus</i> CO2+Con	Isolates the climate response to enhanced 50% LAI, excluding the direct radiative and reduced stomatal conductance effects
BioPhys	CO2+LAI <sub>50</sub> +Con <i>minus</i> CO2_only	Isolates the combined vegetation biophysical effects of reduced conductance and enhanced 50% LAI
AlIEffects	CO2+LAI <sub>50</sub> +Con <i>minus</i> Baseline	Includes all the effects/forcings tested, i.e. the combined radiation, reduced stomatal conductance, and enhanced 50% LAI effects
LAI <sub>CMIP</sub> _Only <sup>a</sup>	CO2+LAI <sub>CMIP</sub> + Con <i>minus</i> CO2+Con	Isolates the climate response to “pseudo” 2xCO <sub>2</sub> LAI, excluding the direct radiative and reduced stomatal conductance effects
BioPhys <sub>CMIP</sub> <sup>a</sup>	CO2+LAI <sub>CMIP</sub> + Con <i>minus</i> CO2_only	Isolates the combined vegetation biophysical effects of reduced conductance and “pseudo” 2xCO <sub>2</sub> LAI
AlIEffects <sub>CMIP</sub> <sup>a</sup>	CO2+LAI <sub>CMIP</sub> + Con <i>minus</i> Baseline	Includes all the effects/forcings tested, i.e. the combined radiation, reduced stomatal conductance, and “pseudo” 2xCO <sub>2</sub> LAI effects

<sup>a</sup>Results shown and discussed in Section 3.6, in comparison to enhanced 50% LAI experiments.

arise between the physical response to radiative forcing of high CO<sub>2</sub> forcing and the vegetation response to higher CO<sub>2</sub> (i.e., the nonlinear radiative-vegetation effects), which we account for and discuss in Section 3.4. Unless otherwise specified in our Results section, a Student’s t-test was used to assess statistical significance, with the sample size modified for temporal autocorrelation where necessary following the methods of Zwiers and von Storch (1995).

We note that the regional Con\_Only responses are also dependent on the photosynthetic pathway of the underlying vegetation, and that C<sub>3</sub>-type vegetation growth is generally more sensitive and responsive to higher CO<sub>2</sub> compared C<sub>4</sub> vegetation (ModelE distribution shown in Figure S19). This distinction may have implications for the magnitude and sign of the hydroclimate responses in regions dominated by C<sub>4</sub> vegetation. Unless otherwise specified, all variables represent 50-year climatological anomalies for the summer growing season: June-August in the Northern Hemisphere, and December-February in the Southern Hemisphere.

### 3. Results and Discussion

#### 3.1. Overall Contributions of BioPhys to AlIEffects

The combined impacts of vegetation and radiative CO<sub>2</sub> effects (“AlIEffects”) result in widespread warming (Figure 2a) and soil moisture drying (Figure 2b).

For many regions, the combined vegetation effects (“BioPhys”, i.e., the combined conductance and LAI effects, Table 2) represent a substantial proportion of the total AlIEffects response (Figures 2c and 2d). Across the northern mid-latitudes and northeastern Australia, BioPhys accounts for 10%–40% of the warming response (Figure 2c), though the vegetation acts to attenuate total warming over some small regions (India, Southeast Asia). BioPhys also contributes a substantial fraction (in some cases, nearly 50%) of the AlIEffects soil moisture responses (Figure 2d), especially over the southwestern US, Iberian Peninsula, Middle East and Central Asia, isolated areas in East Asia, and central and eastern Australia where soil moisture losses are pervasive. BioPhys partially ameliorates (and in some cases, reverses) soil moisture losses across central

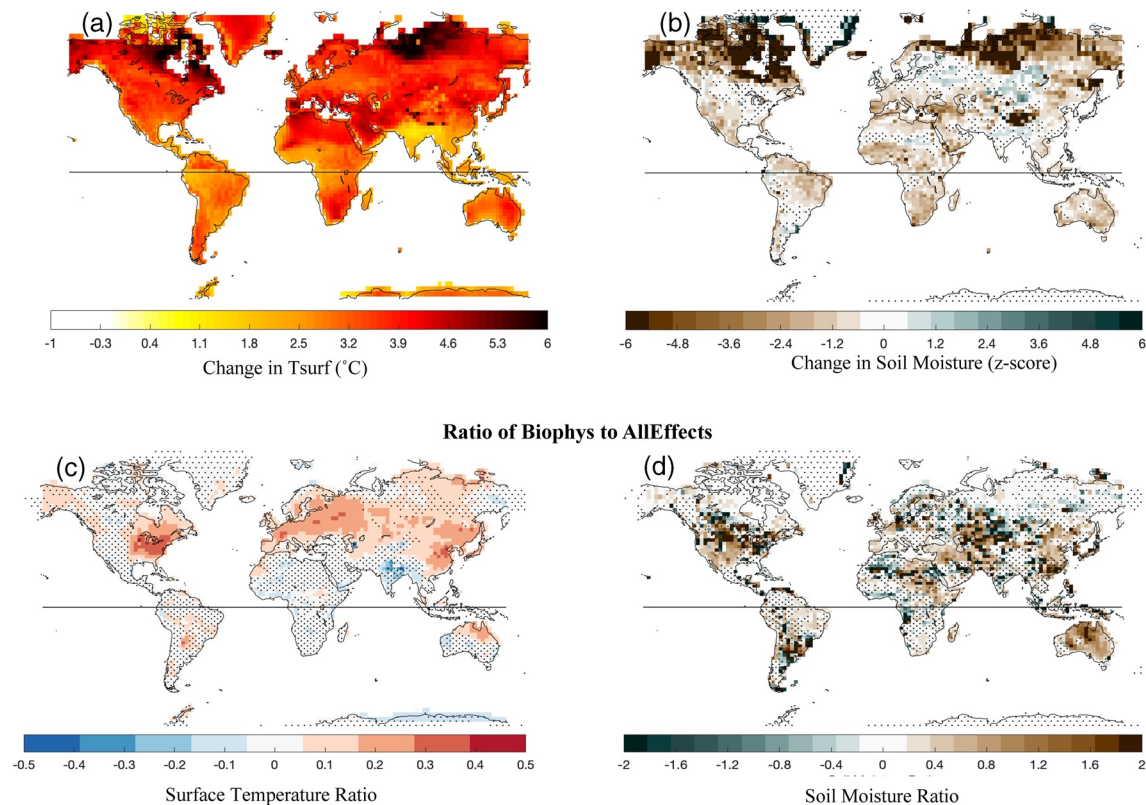


**Figure 2.** AlIEffects responses (measured against Baseline as in Table 2) for (a) surface temperature ( $^{\circ}\text{C}$ ) and (b) soil moisture difference (top 57 cm), normalized by standard deviation of the reference experiment in Table 2 (z-score). This unit is used for all subsequent soil moisture anomalies shown herein. Stippling indicates responses are not significant via a Student's  $t$ -test ( $p < 0.05$ , sample size adjusted for autocorrelation where relevant). The ratio of Biophys to AlIEffects to a doubling of  $\text{CO}_2$  for (c) surfacetemperature and (d) soil moisture, shown for Biophys significant gridcells. All responses shown for hemisphere-respective growing seasons.

Canada and central Asia – areas situated in transition zones from moisture to energy-limited domains. Attenuated soil moisture losses are also present in western Africa and along the southern Pampas in Argentina. More broadly, however, the sign of the Biophys impacts is consistent with the AlIEffects response, indicating that for most areas the aggregate vegetation impacts amplify regional climate changes from  $\text{CO}_2$  radiative forcing.

### 3.2. Rad\_Only: Climate-vegetation Responses to Enhanced Radiative Forcing Under High $\text{CO}_2$

Rad\_Only drives a strong and significant land surface warming during each hemisphere's respective summer season (Figure 3a), forced by increases in net surface radiation and enhanced net longwave radiation at the surface (SI Figures 1b and 1d), with likely contributions from teleconnections due to oceanic warming in remote locations (not shown) (Byrne & O'Gorman, 2013; Joshi et al., 2008).

Land surface warming causes widespread reductions in soil moisture (Figure 3b), especially at high northern latitudes, in the tropics, and in water-limited regions like central California, coastal Australia, and the Mediterranean. For some regions (e.g., tropical South America, the Mediterranean, western and southern Africa), the soil moisture drying is associated with precipitation declines. Soil moisture drying is nevertheless more widespread and also occurs in some regions with precipitation increases (particularly in the Northern Hemisphere). The widespread drying is a response to transpiration, as well as bare soil evaporation, increases as radiation-induced warming increases atmospheric water demand (shown as vapor pressure deficit, VPD, in SI Figure 1a). Over much of the high-latitude land areas, for example, these changes combine to drive widespread soil moisture losses (Figure 3b) despite enhanced precipitation (Figure 3c). Some regions see little change or small increases in soil moisture, namely mid-latitude Central Asia, North

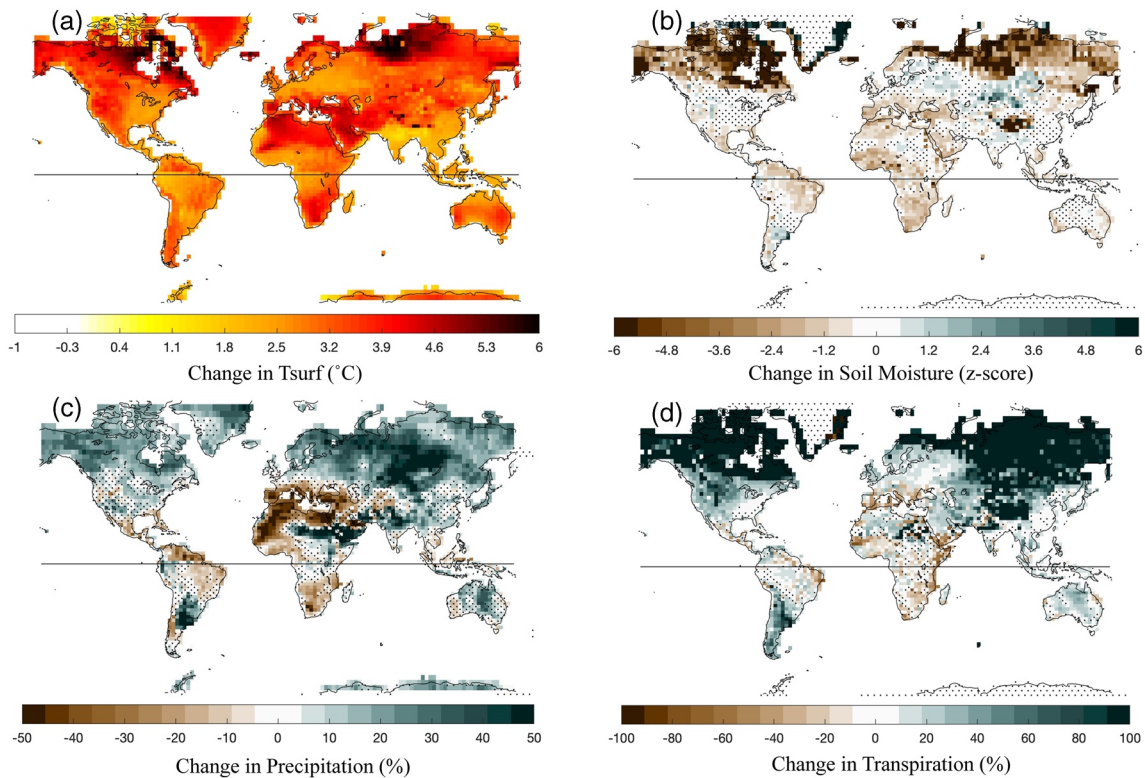


**Figure 3.** Change in growing season (a) surface temperature, (b) soil moisture (top 57 cm), (c) precipitation, and (d) transpiration due to Rad\_Only effect. Stippling indicates responses are not significant via a Student's *t*-test ( $p < 0.05$ , sample size adjusted for autocorrelation where relevant).

America, southeastern South America, and along the Indo-Gangetic Basin. This may be partly due to slightly enhanced precipitation over these regions that is a consequence of circulation changes and higher moisture convergence (Figure 3c), which has also been documented by previous studies (e.g., Chadwick et al., 2019). These precipitation increases lead to slight gains in soil moisture, despite increases in transpiration (Figure 3d). Locations where transpiration declines are where precipitation reductions drive strong soil moisture declines, such as the Mediterranean.

### 3.3. Con\_Only: Climate Responses to Reduced Stomatal Conductance Response Under High CO<sub>2</sub>

Zonally averaged (land only) anomalies shown in Figure 4 for soil moisture (Figure 4a), precipitation (Figure 4b), and temperature (Figure 4c) provide a direct global-scale comparison of the Con\_Only, LAI\_Only, and BioPhys effects. We also provide their geographic distributions (shown as maps in Figures 5 and 6) to determine which regions and hydroclimate regimes are most impacted and/or dominate the fully-coupled response.

In the zonal mean, Con\_Only produces small but positive soil moisture anomalies across the tropics and subtropics between 20°S and 35°N, and at higher southern latitudes dominated by a few gridcells in Patagonia (Figure 4a, red line). Across the mid-latitudes in the Northern Hemisphere, however, Con\_Only results mitigate soil moisture declines. Regionally (Figure 5a), Con\_Only produces slight but significant increases in soil moisture across southern South America (which dominates the zonal mean), the Indian peninsula, and western and central Africa. Significant soil moisture increases are also present at depth (SI Figures 3a and 3d). No significant soil moisture anomalies are present across several other water-limited regions, including southern Europe and the American Southwest. Slight decreases in soil moisture are distributed across eastern Australia and the northern mid-to-high latitudes, including large portions of Canada, Central Asia, and eastern Asia (Figure 5a, SI Figures 3a and 3d).

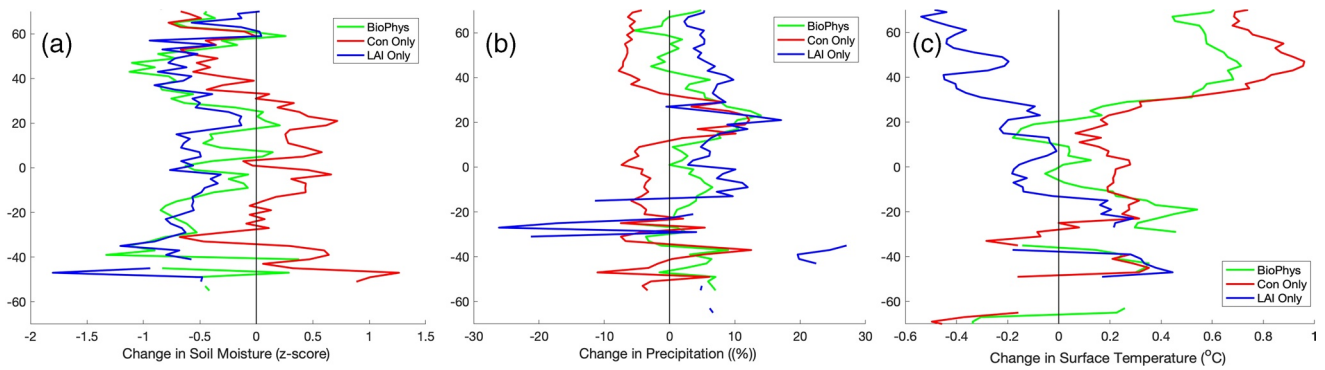


**Figure 4.** Zonally averaged growing season anomalies for (a) soil moisture for top 57 cm, (b) precipitation, and (c) surface temperature for BioPhys effect (green), Con\_Only (red), and LAI\_Only (blue). Only significant gridcells (via a Student's *t*-test described in the Methods section) were used in the creating the zonal average.

One would naively expect reducing conductance to increase soil moisture, but several of the areas that show declines in soil moisture in Con\_Only have declines in precipitation (Figure 5d) that dominate the zonal averages (Figure 4b). Some areas where precipitation decline are characterized by atmospheric conditions that are less conducive to precipitation. For example, Con\_Only shows a strong and significant reduction in relative humidity (Figure 7a) in the northern mid-to-high latitudes and eastern Asia, predominantly at lower atmospheric levels and in the PBL. The latter also deepens and warms (Figures 7b and 7c), thereby further inhibiting summertime rainfall. We note that this result could be model dependent, for example related to model PBL representations (C. M. Taylor et al., 2012), and that previous studies have shown differing precipitation responses to vegetation changes under high CO<sub>2</sub>.

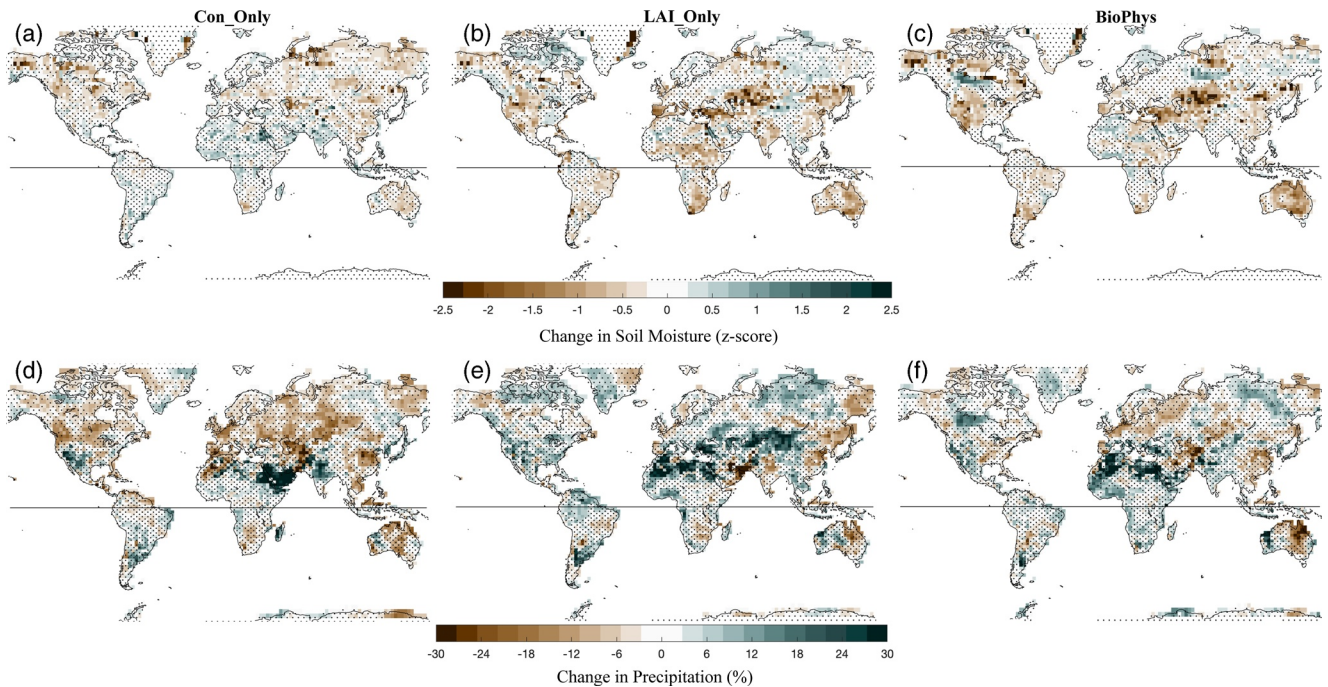


**Figure 5.** 50-years climatological growing-season anomalies. Row 1: soil moisture (z-score, top 57 cm) for Con\_Only (a), LAI\_only (b), and Biophys (c). Row 2: precipitation for Con\_Only (d), LAI\_only (e), and Biophys (f). Anomalies are shown for each hemisphere's respective summer. Stippling indicates responses are not significant via a Student's *t*-test ( $p < 0.05$ , sample size adjusted for autocorrelation where relevant).

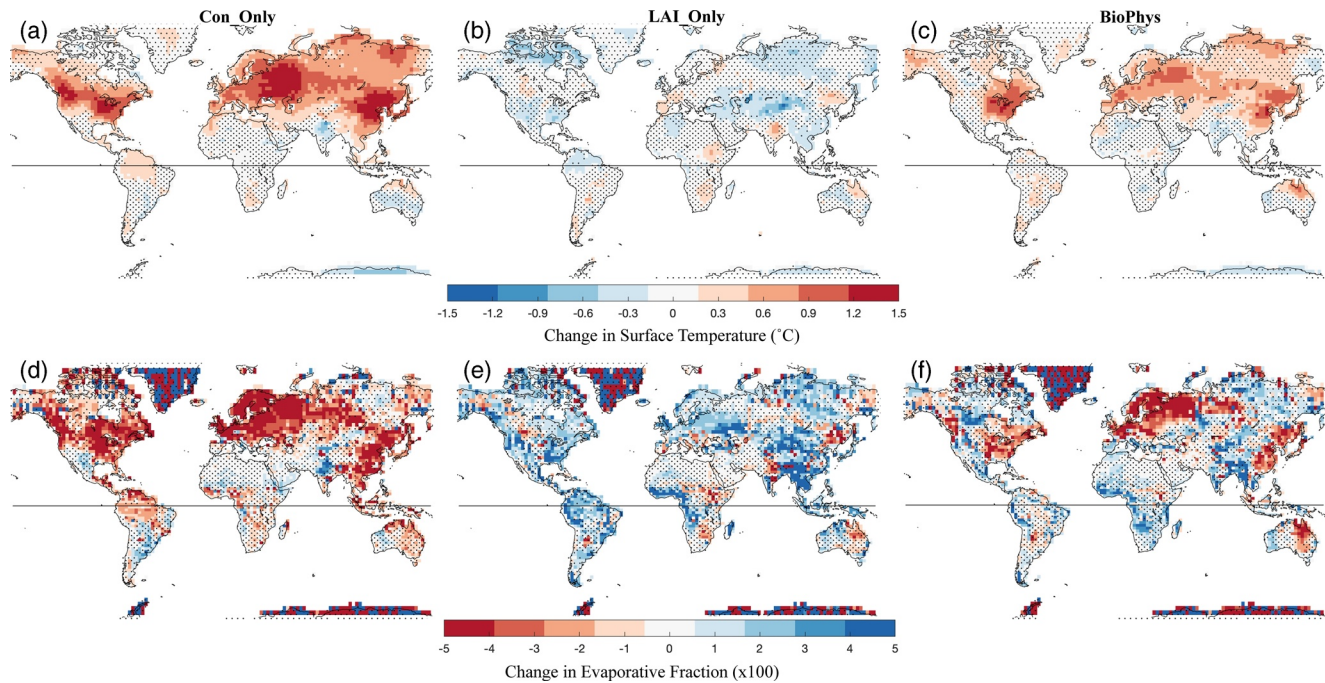


**Figure 6.** 50-years climatological growing-season anomalies. Row 1: surface temperature ( $^{\circ}\text{C}$ ) for Con\_Only (a), LAI\_only (b), and Biophys (c). Row 2: evaporative fraction ( $\times 100$ ) for Con\_Only (d), LAI\_only (e), and Biophys (f). Anomalies are shown for each hemisphere's respective summer. Stippling indicates responses are not significant via a Student's  $t$ -test ( $p < 0.05$ , sample size adjusted for autocorrelation where relevant).

For example, Skinner et al. (2017) highlight how reduced stomatal conductance forces a warming and drying (i.e. reduced relative humidity) of the PBL, which can reduce low cloud cover and increase the number of dry days during the growing season in the mid-latitudes. Furthermore, there is reduced moisture convergence over East Asia under Con\_Only conditions (SI Figure 5b, brown colors), which could enhance regional precipitation and soil moisture declines. Moisture convergence appears slightly enhanced (SI Figure 5b) over the US Midwest and northeastern Asia, although given the enhanced atmospheric stability in these regions (Figure 7b), this does not appear to translate into increased precipitation (Figure 4b) and the evaporative fraction (EF), the ratio of latent heat flux to the sum of the turbulent fluxes), is reduced.

The low-level warming and drying in Con\_Only is largely driven by this EF decline (Figure 6d), indicating a reduced proportion of surface energy partitioned to latent heat fluxes. There exists a close geospatial relationship between the EF and surface temperature response patterns that are overall consistent with the zonally averaged surface temperature anomalies. Con\_Only produces a pronounced warming at mid-to-high latitudes by nearly  $1^{\circ}\text{C}$ , and substantially less warming across the sub-tropics and tropics.

A unique response to Con\_Only occurs over South Asia along the western Indo-Gangetic Basin: an increase in soil moisture, precipitation, runoff (SI Figure 4b), and evaporative fraction co-located with small, but significant, reductions in surface temperature (Figures 5a–5d). The latter may be largely a result of the enhanced EF (Figure 6d) that increased partly as a result of the regionally enhanced rainfall. Additionally, South Asia is one of the few regions under Con\_Only conditions that also shows a slight shallowing of the PBL (Figure 7b), partly resulting from the regional cooling, and increased atmospheric moisture convergence (SI Figure 5b). While somewhat counterintuitive, this result is consistent with previous findings that also suggest higher rainfall and cooler temperatures in India as an indirect consequence of biophysical vegetation feedbacks on regional atmospheric circulation and moisture transport (Douvillle et al., 2000; Skinner et al., 2017). This Con\_Only response may also amplify the precipitation increases that result from Rad\_Only-induced circulation changes (Figure 3c). Large percent increases in precipitation also result across the Middle East and over the central Argentine grasslands (Figure 5d), although we note that these increases are not as large in absolute terms given the relatively water-limited conditions.

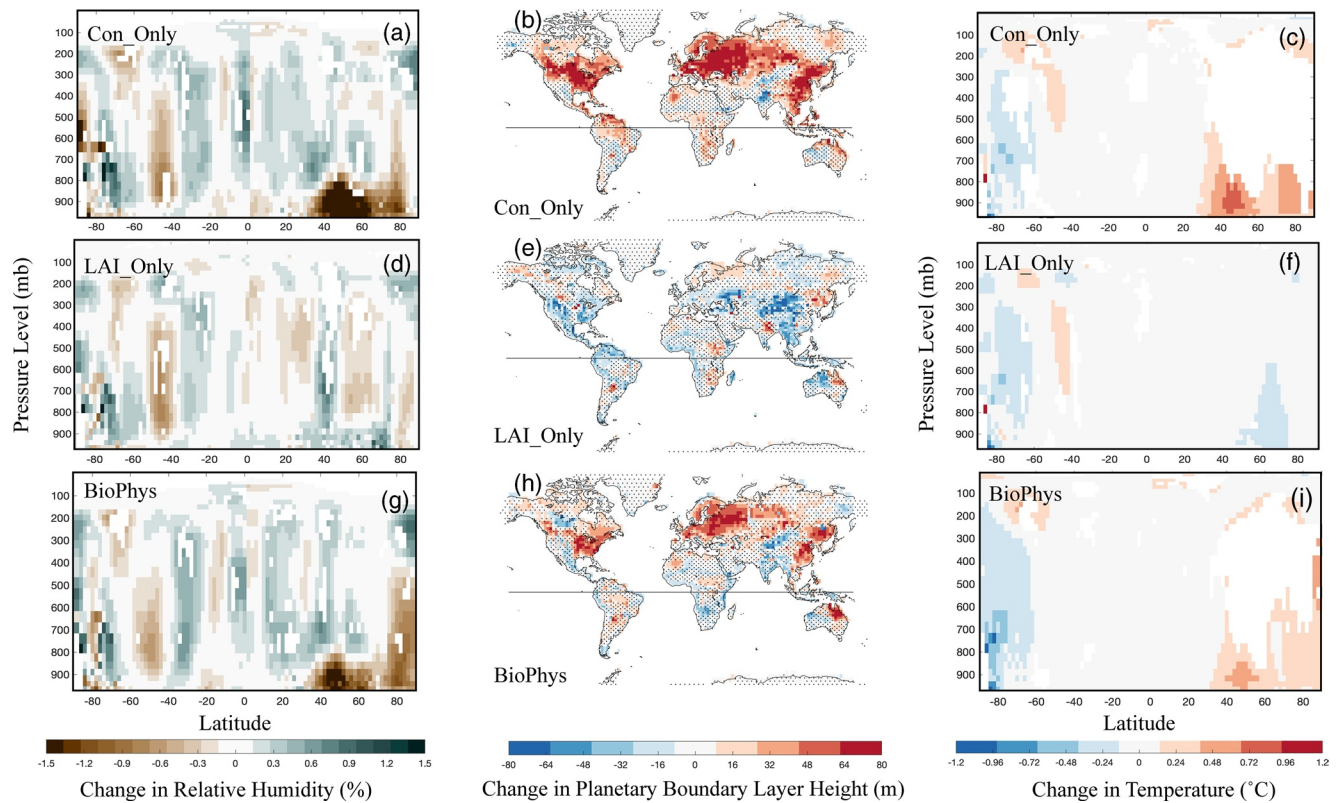


**Figure 7.** Row 1 shows Con\_Only growing season changes in (a) pressure level  $\times$  latitude relative humidity, (b) depth of the planetary boundary layer (m), and (c) pressure level  $\times$  latitude change in temperature. Similarly, Row 2 shows respective changes in these variables for LAI\_Only, and Row 3 for BioPhys. Stippling indicates responses are not significant via a Student's t-test ( $p < 0.05$ , sample size adjusted for autocorrelation where relevant).

### 3.4. LAI\_Only: Climate Responses to Enhanced LAI Under High CO<sub>2</sub>

The climatic responses resulting from enhanced LAI generally oppose those of the Con\_Only effect. Enhanced LAI consistently reduces mean zonal soil moisture across all latitudes (Figure 4a, blue line) while also increasing zonal mean precipitation (albeit less consistently, Figure 4b). Soil moisture losses are particularly strong across more water-limited environments, such as western North America, southern Europe and the Mediterranean region, Central Asia, eastern Asia, Sahelian Africa, peninsular South Asia/India, and eastern Australia (Figure 5b), and continue through one and 2 meter depths (SI Figures 3d and 3e). In some areas, such as eastern Australia, eastern Asia, Sahelian Africa, and the US Southwest, soil moisture losses also increase at greater depths.

In parts of Central Asia and West Africa, soil moisture losses occur despite small increases in precipitation (less than or  $\sim 20\%$ ) (Figure 5e). Over Central Asia, increases in precipitation may be facilitated by a relative moistening of the overlying atmosphere (Figure 7d) and reduced PBL height (Figure 7e; temperature changes are otherwise mostly negligible in Figure 7f). It is also possible that these regional increases in precipitation result partly from enhanced local contributions, such as greater terrestrial moisture recycling from LAI-related transpiration increases, as there is no strong indication of greater moisture convergence in many of these areas (Figure SI5c). In fact, recent observational studies show higher ET fluxes associated with significant greening coincide with increasing precipitation trends, suggesting that enhanced local moisture recycling may be playing an important role despite remaining uncertainties in understanding of this process (Zhang et al., 2015). Over South Asia, reductions in moisture convergence (Figure SI4c) may contribute to isolated precipitation declines over northeastern Indo-Gangetic Basin (Figure 5e) and co-located soil moisture losses (Figure 5d).

More generally, soil moisture losses are likely driven by the overall strong increases in EF, particularly across most tropical to mid-latitude regions (Figure 6e), although we note that these changes are weaker in

magnitude compared to the EF reductions in the Con\_Only experiment (Figure 6d). Across many sub-tropical and low-latitude areas, heightened EF results in a weak but significant cooling (Figure 6b), although there are some exceptions. For example, despite increases in EF across South America and southern Africa, the overall thermal response of enhanced LAI south of the equator is a slight warming (Figure 4c), which contrasts with both the Con\_Only and BioPhys effects (the latter described below). However, these zonally averaged responses are dominated by a weak warming over eastern Australia (Figure 6b), resulting from a greater partitioning of the surface energy balance toward sensible heat fluxes (i.e., reduced EF, Figure 6d). In the Northern Hemisphere, LAI\_Only results in a slight but significant cooling (Figure 6b) and strong EF increase that are most prevalent across the northern sub-tropics and lower mid-latitudes (Figure 6d).

In northeastern Australia, strong soil moisture losses are widespread despite more isolated areas of reduced EF (Figure 6d) and precipitation (Figure 5e). Changes in the low-level relative humidity are also mostly negligible in the Southern Hemisphere sub-tropics (Figure 7d). However, warmer surface temperatures in this region (Figure 6b), which partly drive increased PBL heights in isolated areas (Figure 7e) and persistent water limitation throughout the year (not shown) serve to amplify regional soil moisture losses. Therefore, despite higher LAI, overall reductions in moisture availability limit evaporative increases in this region. Lastly, we note that northeastern Australian is characterized by large fractions of  $C_4$  vegetation (Figure SI9) that is expected to be less responsive to enhanced  $CO_2$  in the short term, although interestingly stronger responses have been documented on longer timescales (Reich et al., 2018).

### 3.5. BioPhys: Non-radiative Climate Responses to Combined Reduced Stomatal Conductance and Enhanced LAI Under High $CO_2$

#### 3.5.1. Prevailing BioPhys Global and Regional Climate Responses

In general, BioPhys soil moisture (Figures 4a and 5c) and precipitation (Figures 4b and 5f) anomalies appear most similar to those of LAI\_Only with respect to both their zonally averaged signs of change and their geographic pattern, particularly at low latitudes and at depths of one and 2 m (SI Figures 3c and 3f) where soil moisture losses are also generally larger. Across southern Central Asia, far East Asia, eastern Australia, the central US, and generally in more water-limited areas, the combined reduced stomatal conductance and enhanced LAI effects produce amplified soil moisture losses compared to either of these effects alone (Figures 5a–5c). In contrast, on the Indian peninsula, soil moisture increases under Con\_Only oppose decreases under LAI\_Only to result in a negligible BioPhys soil moisture response.

Zonally averaged BioPhys precipitation responses are generally small relative to the other experiments due to partial cancellation of the effects of LAI by those of conductance (Figure 4b). At higher latitudes over Europe, BioPhys produces precipitation declines that are similar to, but smaller than, those of Con\_Only and broadly coincident with reductions in moisture convergence (SI Figure 5d). Across sub- and semi-arid tropics, particularly West Africa, BioPhys increases in precipitation are similar to those in LAI\_Only. These results suggest that the enhanced LAI effect may significantly influence the overall hydrological response under high  $CO_2$  in more water-limited regions, but there are important uncertainties surrounding constraints on LAI growth in these regions (Pu & Dickinson, 2014; Skinner et al., 2018; Swann, 2018).

BioPhys surface energy partitioning and thermal responses resemble those of Con\_Only (Figures 6f and 6c), though muted, and the strongest anomalies are found in the Northern Hemisphere mid-latitudes. Specifically, BioPhys displays strong and significant EF reductions (Figure 6f) across these regions, including eastern North America, western and northern Europe, far eastern Asia, and northeastern Australia, although these declines appear regionally attenuated by LAI\_Only EF patterns (Figure 6d). These EF declines are accompanied by strong and significant surface temperature increases (again, somewhat ameliorated by LAI\_Only cooling where present) that closely track Con\_Only anomalies (Figures 6c and 7i). These regional temperature anomalies, ranging from 0.5°C to 1.5°C (Figure 6c compared to Figure 6a), also partly drive a deeper PBL (Figure 7h). These responses, combined with reductions in both relative humidity at lower levels (Figure 7g) and moisture convergence (SI Figure 5d), help explain the modest precipitation reductions over Europe and Australia. We also note that across tropical and sub-tropical (e.g., monsoon) regions, BioPhys shows EF increases (Figure 6f) similar to LAI\_Only, although of reduced magnitude. In the US

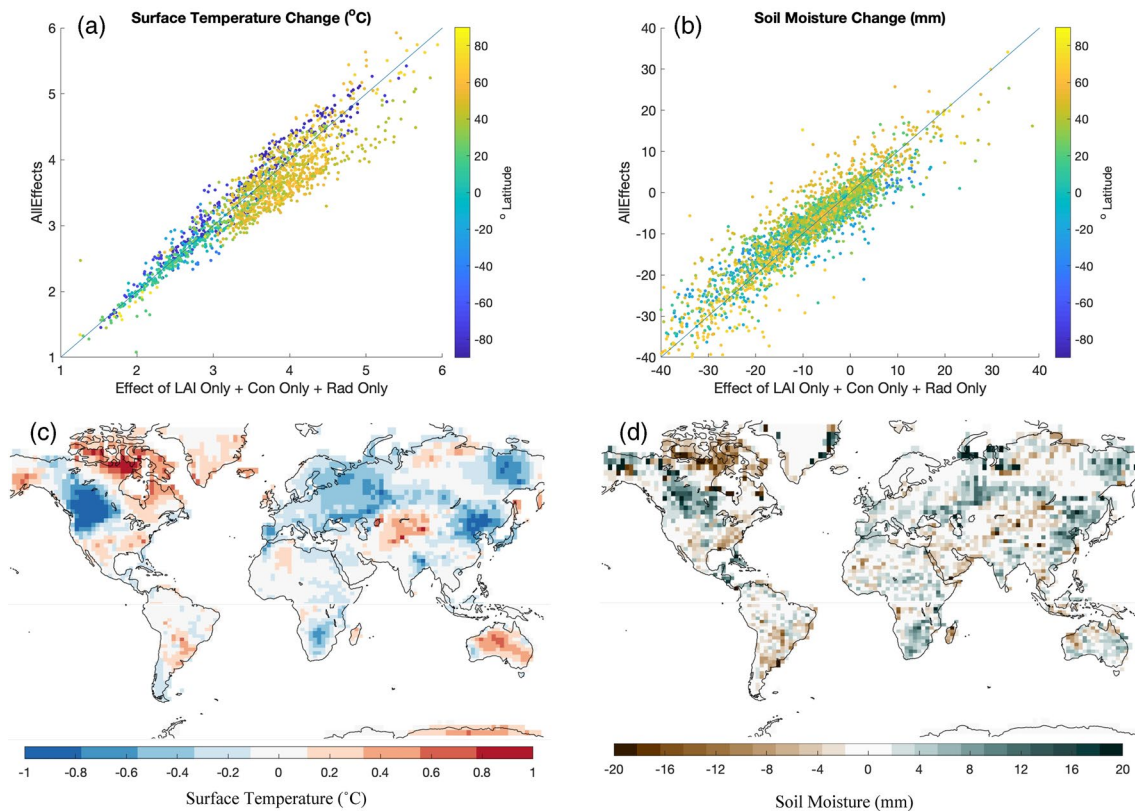


**Figure 8.** AllEffects versus the combined LAI\_Only + Con\_Only + Rad\_Only effect for growing season (a) surface temperature ( $^{\circ}\text{C}$ ), and (b) soil moisture (mm, top 57 cm). A perfect correspondence between the AllEffects response and LAI\_Only + Con\_Only + Rad\_Only response would fall on the 1:1 line shown on the figures. The geographic distribution of the nonlinear interaction term, taken as AllEffects - (RadOnly + LAIonly + ConOnly), for (a) surface temperature and (b) soil moisture during the growing season.

Southwest and Iberian Peninsula, these EF increases contribute to regional soil moisture losses, despite co-located areas of increased rainfall, via processes similar to those described for LAI\_Only above.

These results are consistent with prior findings suggesting that enhanced LAI under elevated  $\text{CO}_2$  exacerbates regional soil moisture declines despite reduced stomatal conductance: a simultaneous “greening but drying” (Mankin et al., 2017). These EF increases result in mostly insignificant temperature changes or a very slight cooling that in some areas, like northern portions of the Amazon basin, offset a slight warming under Con\_Only. In general, the Con\_Only warming appears to dominate the mid-to-high latitude climate response under BioPhys conditions, although it is somewhat attenuated by enhanced LAI.

Northeastern Australia is among the few regions characterized by both a significant warming and drying (soil moisture losses in Figure 5c) that appears to result from mutually amplifying Con\_Only and LAI\_Only effects. Northeastern Australian precipitation declines are accompanied by reduced regional EF (Figure 6d–6f) and slight increases in surface temperature (Figure 6c). The latter further contributes to increased PBL heights (Figure 7h) and, coupled with the slight low-level drying in the subtropics of the Southern Hemisphere (Figure 7g, around  $20^{\circ}\text{S}$ ), inhibits rainfall. With reduced rainfall and higher atmospheric water demand with warmer temperatures (Figure 6c), the combined conductance and LAI effects lead to amplified regional drying (Figure 5c).

### 3.5.2. Evaluating Nonlinearities in the Combined AllEffects Climate Responses

We further consider how the addition of the isolated Rad\_Only, LAI\_Only, and Con\_Only effects compares to the total, interactive AllEffects response. Due to our experimental design, we note that we evaluate the nonlinearity between enhanced LAI and reduced conductance, but not explicitly the nonlinearities with radiation. This analysis is shown in two ways in Figure 8.

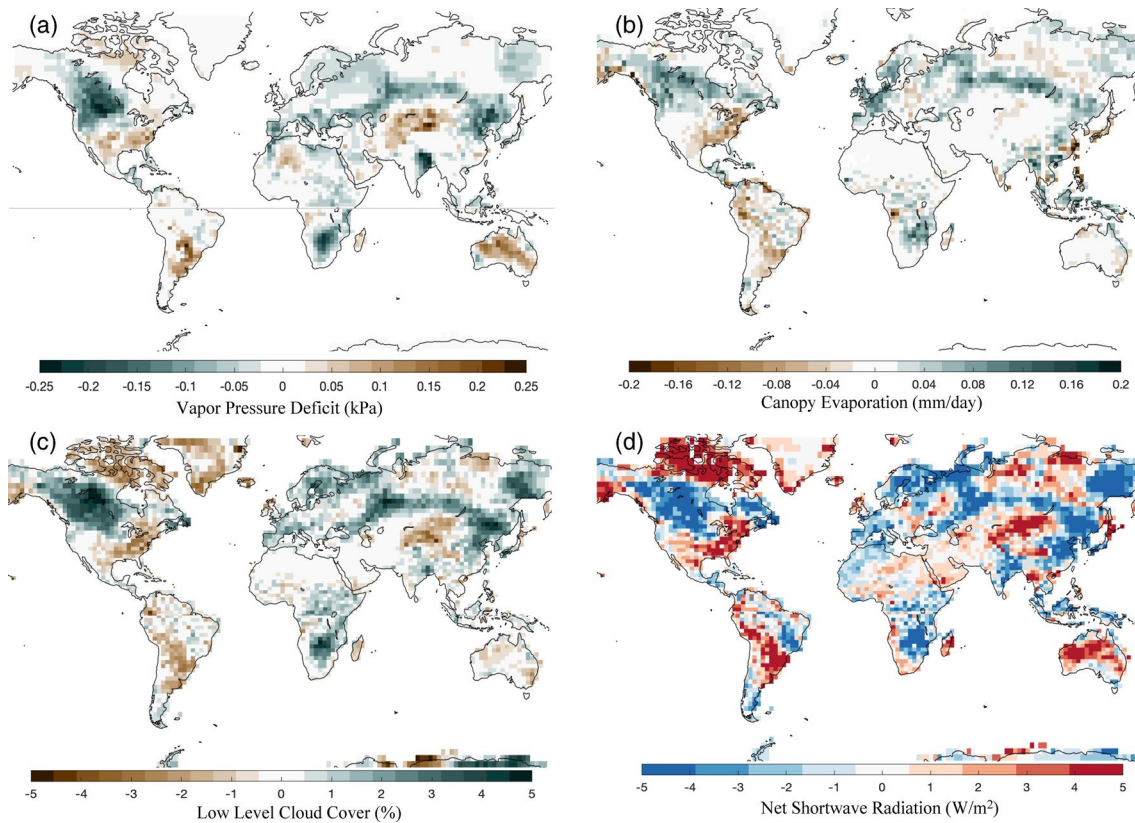


**Figure 9.** The geographic distribution of the growing season nonlinear interaction term, taken as  $\text{AllEffects} - (\text{RadOnly} + \text{LAIonly} + \text{ConOnly})$ , for (a) vapor pressure deficit, and (b) canopy evaporation, (c) low level cloud cover, and (d) net shortwave radiation.

In Figures 8a and 8b, where each point represents the response per land grid cell, a perfect correspondence between the AllEffects and  $\text{LAI}_{50\_Only} + \text{Con\_Only} + \text{Rad\_Only}$  effects would fall on the 1:1 line, and departures from this line indicate the influence of nonlinear interactions between enhanced radiative forcing, higher LAI, and reduced conductance under AllEffects conditions. The geographic distribution of the nonlinear terms ( $\text{Nonlinear Term} = \text{AllEffects} - (\text{Rad\_Only} + \text{LAI}_{50\_Only} + \text{Con\_Only})$ ) following the approach of Skinner et al. (2017) are shown in Figures 8c and 8d. In general, AllEffects shows attenuated warming relative to the combined  $\text{LAI}_{50\_Only} + \text{Con\_Only} + \text{Rad\_Only}$  effects, particularly at higher temperature increases (e.g.,  $>0.5^\circ\text{C}$ , Figure 8a) and at high latitudes in Eurasia (e.g.  $40^\circ\text{N}$ – $80^\circ\text{N}$ ). At lower latitudes, AllEffects temperature responses are more distributed across the 1:1 line. In contrast, the soil moisture anomalies are largely linearly additive (Figure 8b), with the possible exception of nonlinear attenuation in central northern North America. To further investigate what may drive this nonlinear response, we show the nonlinear effects in the vapor pressure deficit (VPD) and canopy evaporation in Figures 9a and 9b.

The geospatial pattern of nonlinear cooling (Figure 8c) closely aligns with where the nonlinear interaction reduces the VPD (Figure 9a). We postulate that enhanced LAI across these regions increases ET through greater leaf-water interception and, thus, enhanced canopy evaporation. This is broadly supported by Figure 9b, and has been previously highlighted as an important control on transpiration and the stomatal conductance term (Halladay & Good, 2017). We note here that the strength of this effect can be model dependent as there exists a large range in canopy evaporation across models and representations must be further improved (De Kauwe et al., 2013). In our simulations, this enhanced canopy evaporation acts to lower the canopy temperature which in turn decreases the VPD (Figure 9a). The consequence is a relaxed stomatal closure response under combined BioPhys conditions, allowing greater ET and, thus, a nonlinear cooling effect.

Over isolated areas in Central Asia, northern Australia, and eastern North America, there also exists a nonlinear warming effect that amplifies BioPhys temperature anomalies (relative to the discrete addition

of the effects). These areas also coincide with increased VPD, via nonlinear interactions, and reduced canopy evaporation (Figures 9a and 9b). Such evaporation reductions, alongside declines in low-level relative humidity (SI Figure 6c), may provide a mechanism for this warming by driving co-located reductions in low-level cloud cover (Figure 9c) and enhanced net shortwave radiation at the surface (Figure 9d).

The ameliorated soil moisture losses shown in Figure 8b are also largely driven by nonlinear effects in the mid-to-high latitudes in central North America, in the Iberian peninsula, far east Asia, and parts of eastern Australia (Figure 8d). At higher latitudes in North America, attenuated soil moisture losses may result from nonlinear effects that increase regional precipitation (SI Figure 6a), which may be partly fueled by in-situ increased canopy evaporation via enhanced LAI (Figure 9b).

Lastly, we provide a further comparison of just the BioPhys effect to the linear addition of Con\_Only and LAI\_Only (“Con\_Only + LAI\_Only”) in SI Figure 10. At higher latitudes, BioPhys warming (SI Figure 10a) is less than Con\_Only + LAI\_Only effects, similar to the AllEffects responses in Figure 8a. Soil moisture responses (SI Figure 10) are more distributed across the 1:1 line, but BioPhys generally appears to produce less severe soil moisture losses compared to the Con\_Only + LAI\_Only effects.

### 3.6. Comparison Between 50% LAI Increases and “Pseudo” $2\times\text{CO}_2$

The sign of LAI change is generally consistent across the CMIP6 models used here and is generally positive globally and in regions displaying the strongest responses. Most models show the strongest positive LAI increases across the mid- and high-latitude regions and over the Amazon, which range widely from  $\sim 30\%$  to upwards of  $100\%$  (SI Figure 7). Regionally, however, some distinctions arise between these models’ responses, particularly across the mid-to-lower latitudes in the US Southwest, Central America, Sahelian Africa, and Australia. We provide a more complete description of these difference in the Supplementary Information section and SI Figure 7.

In general,  $\text{LAI}_{2\times\text{CO}_2\text{-only}}$  responses (SI Figure 8) closely resemble those of LAI\_only (Figures 5 and 6, column 2) in both magnitude and geospatial distribution. The most notable differences occur in the precipitation fields (SI Figures 8b and 8e), namely in that positive precipitation anomalies along the West African coast in LAI\_Only are absent in  $\text{LAI}_{2\times\text{CO}_2\text{-only}}$ .

Likewise, the contribution of  $\text{BioPhys}_{\text{CMIP}}$  to  $\text{AllEffects}_{\text{CMIP}}$  (Figures 10a and 10b) are consistent with BioPhys to AllEffects (Figures 2c and 2d). In particular,  $\text{BioPhys}_{\text{CMIP}}$  exhibits the strongest contributions to the  $\text{AllEffects}_{\text{CMIP}}$  surface temperature response (Figure 10a) in the eastern US, Europe, and East Asia. Furthermore,  $\text{BioPhys}_{\text{CMIP}}$  contributes a moderate warming to  $\text{AllEffects}_{\text{CMIP}}$  at higher latitudes in Russia, which was not present in BioPhys.  $\text{BioPhys}_{\text{CMIP}}$  also contributes more strongly to the cooling shown over northern South Asia and more widespread warming over Australia relative to BioPhys. Likewise,  $\text{BioPhys}_{\text{CMIP}}$  contributions to  $\text{AllEffects}_{\text{CMIP}}$  soil moisture changes (Figure 10b) are generally of similar magnitude to BioPhys:AllEffects across most regions, and particularly in regions with the strongest responses in Figure 2d: US Southwest, Central Asia, parts of East Asia, and Australia. Departing from these similarities, however,  $\text{BioPhys}_{\text{CMIP}}$  displays small, positive contributions to  $\text{AllEffects}_{2\times\text{CO}_2}$  soil moisture responses in southern Africa (Figure 10b). Here the “pseudo”  $2\times\text{CO}_2$  LAI increases are slightly less widespread and there also exist a few grid cells with small declines (Figures 1b and 1c). These small differences in the imposed LAI change may reduce transpiration losses that are observed in LAI\_Only and elsewhere under the “pseudo”  $2\times\text{CO}_2$  conditions.

Overall, the  $\text{AllEffects}_{\text{CMIP}}$  nonlinear surface temperature responses (Figure 10c) are stronger than those of AllEffects. While the geospatial pattern of these responses are generally similar, some regional distinctions emerge. For example,  $\text{AllEffects}_{\text{CMIP}}$  shows more pronounced nonlinear cooling effects in the upper mid-latitudes and toward the northern Midwest, while its western European response is diminished in comparison to AllEffects. In notable contrast to AllEffects,  $\text{AllEffects}_{\text{CMIP}}$  produces a moderate nonlinear warming in far East Asia at the lower midlatitudes. Common to both  $\text{AllEffects}_{\text{CMIP}}$  and AllEffects are positive nonlinear soil moisture effects in the northern Great Plains (Figures 10d and 8d, respectively), although the  $\text{AllEffects}_{\text{CMIP}}$  responses do not extend as far northward and in general both experiments show much spatial heterogeneity.

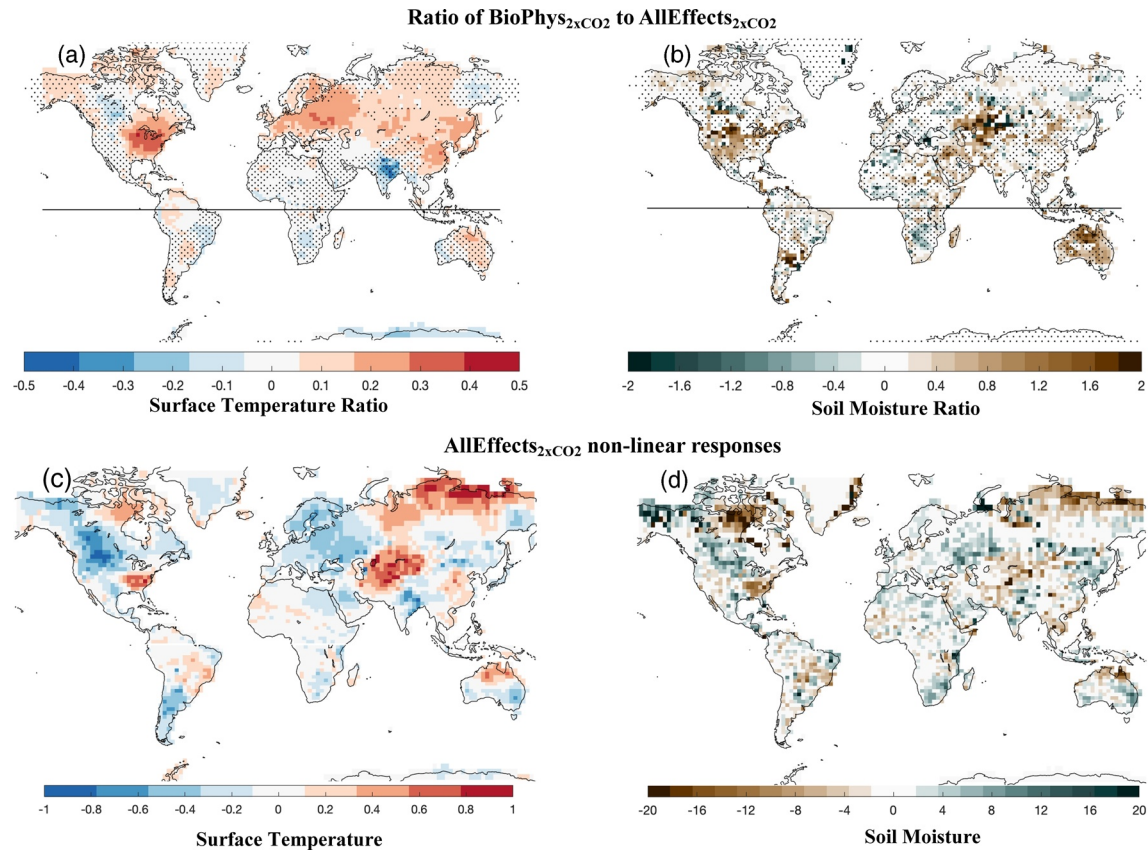


**Figure 10.** Growing season responses for experiments prescribed with LAI from “pseudo” 2xCO<sub>2</sub> experiment. Ratio of BioPhys to AllEffects for (a) surface temperature and (b) soil moisture for top 57 cm. AllEffects non-linear responses (as computed in Section 3.5) for (c) surface temperature (native unit °C) and (d) soil moisture for top 57 cm (native unit mm).

We further contextualize our results by comparing them (primarily using our 50% LAI increase experiments) to CMIP model analyses undertaken in previous work. For example, Lemordant et al. (2017) evaluated the vegetation response (“PHYS”) to increasing 1% per year CO<sub>2</sub> forcing, “1pctCO<sub>2</sub>”, for a six-model ensemble from the Fifth Coupled Model Intercomparison Project (CMIP5, K. E. Taylor et al., 2012). These experiments isolated the vegetation physiological response, which accounted for both changes to LAI and conductance combined, from the radiation response. Lemordant et al.’s PHYS can be qualitatively compared to our BioPhys results (notwithstanding the differences in our experimental design). Their results show that the modeled vegetation response to high CO<sub>2</sub> drives soil moisture losses across many water limited areas, particularly the US Southwest, southern Africa, Australia, and Central Asia (their Figure 2L). These regional responses are also reflected in BioPhys (Figure 5c), although the southern African responses are less widespread. BioPhys results also show broadly similar geospatial patterns of change in the EF (their Figure 2I): PHYS and BioPhys responses both show relatively strong declines in EF along the northwestern and eastern US, Europe, and East Asia. Both responses are also negative over the Amazon, although again the BioPhys response is less widespread.

BioPhys does exhibit positive EF changes in several areas that are not consistent with PHYS, for example in West Africa, Central America, and parts of southeastern Asia (Figure 5f). One possible explanation for this stems from our uniformly applied 50% LAI increase everywhere, which does not represent the distribution of vegetation responses produced by the dynamic vegetation models included in PHYS, or for that matter in our “pseudo” 2xCO<sub>2</sub> LAI. These models tend to display less LAI growth (or even declines) at lower latitudes (e.g. Figures 1b and 1c). In contrast to our 50% LAI increase experiments, we note that LAI<sub>CMIP\_Only</sub> does display more grid cells with EF declines across Central America and West and Sahelian Africa (SI Figure 8c) and is slightly more consistent with PHYS EF. Thus, the larger LAI change prescribed in the 50% LAI experiment may partly account for these regional EF differences between BioPhys and PHYS.

### 3.7. Outstanding Uncertainties and Key Considerations

This study is among the few to explicitly disentangle reduced stomatal conductance and enhanced LAI effects in an ESM and assess their separate and additive effects on climate under high CO<sub>2</sub>. Our results demonstrate that the interactions between these effects are complex, regionally varied, and, critically, not always additive across all areas. As such, these sensitivity experiments highlight key processes and regional responses—namely a warming at high latitudes and drying across water-limited domains—that may aid the development of more comprehensive and dynamic vegetation simulations and facilitate an improved understanding of observed ecosystem changes under rising CO<sub>2</sub>.

Nevertheless, we note some key limitations to this study and uncertainties that warrant additional experimentation. First, our analyses excluded the effects of changing albedo with LAI. However, higher LAI may reduce albedo and thereby enhance net surface shortwave radiation, in isolation from other plant physiological effects and feedbacks (e.g. with clouds). In fact, this LAI-induced albedo effect has been shown to warm energy-limited domains, such as boreal forest regions (Forzieri et al., 2017; Zeng et al., 2017), although its impact is much more limited at lower latitudes where LAI-ET effects dominate. We would therefore expect that including this effect in future simulations would further amplify warming from CO<sub>2</sub> radiative and conductance effects at higher latitudes.

Second, raising LAI by 50% across all vegetation types was intended to test the sensitivity of this component of the vegetation response to large changes. This globally prescribed increase is likely an overestimate, particularly at lower latitudes, as we expect LAI changes to be non-uniform across vegetation types (e.g., species and photosynthetic pathway), stages of growth, bioclimatic zones, and resource limitations (Donohue et al., 2013; Norby & Zak, 2011). While the CMIP6 ensemble used herein generally represented this geospatial heterogeneity, LAI changes in response to high CO<sub>2</sub> forcing also exceeded 50% in some water-limited areas in the lower mid latitudes and at higher latitudes. Satellite-based analyses do suggest that water-limited environments may in fact exhibit a proportionally greater LAI response as a result of enhanced water use efficiency from CO<sub>2</sub> fertilization (Donohue et al., 2013). Meanwhile, FACE experiments indicate a more attenuated LAI increase in response to CO<sub>2</sub> (Betts et al., 1997; Norby & Zak, 2011; Warren et al., 2011). More recently, evidence from a mature *Eucalyptus* woodland showed that LAI was unresponsive to elevated CO<sub>2</sub> (Duursma et al., 2016).

An analysis by Skinner et al. (2018) of CMIP5 ESMs with dynamic vegetation showed their broad consistency with these geographic patterns of LAI change, particularly in semi-arid environments (Skinner et al., 2018). A site-based comparison between FACE experiments and CMIP5 models by Mankin et al. (2019) nevertheless highlights the discrepancies and uncertainties in simulated vegetation responses and key hydrologic trends. Some of these uncertainties stem from imperfect comparisons between FACE experiments and their protocols and transient CMIP5 model experiments. However, more targeted model-observation comparisons of simulated changes in LAI in response to elevated CO<sub>2</sub> at a series of FACE experiments have shown similar errors (De Kauwe et al., 2014, 2016; Medlyn et al., 2015). These challenges in appropriately representing plant physiological responses to climate forcings lead to both process-based uncertainty and also considerable inter-model uncertainty. For example, Mahowald et al. (2016) found large inter-model variation in simulated LAI responses under the Representative Concentration Pathways in CMIP5, which may be partly related to the spread in the models' simulation of precipitation and incorporation of vegetation stress factors related to both water and heat. Comparisons of model LAI to observations are also complicated by the lack of adequate comparison metrics, which poses challenges to model development prospects as well as future LAI projections (Mahowald et al., 2016).

Furthermore, most climate models still lack (or over-simplify) a host of processes that can impose additional limits on the total biophysical vegetation response and result in over-prediction of LAI and/or conductance effects (Swann, 2018). For example, leaf acclimation, or increasing thickness of leaves in response to high CO<sub>2</sub>, can limit and/or negate increases in LAI and result in additional warming over that induced by conductance effects alone (Kovenock & Swann, 2018). Stomatal conductance may also be further reduced by a reduction in the maximum rate of carboxylation ( $V_{c,max}$ ) under high CO<sub>2</sub> (Ainsworth & Rogers, 2007; Kovenock & Swann, 2018; Leakey et al., 2009), although the contribution of this effect remain uncertain (Ainsworth & Rogers, 2007). Prior model studies scaled  $V_{c,max}$  to approximate this effect

(Bounoua et al., 2010; Pu & Dickinson, 2014), which resulted in ET reductions that further amplify directly induced plant physiological temperature increases (Pu & Dickinson, 2014). On the other hand, if the additional water savings from down-regulated  $V_{c,max}$  are instead partitioned to higher LAI (over and above direct CO<sub>2</sub>-physiological effects), the resultant cooling may compensate for the warming effects of reduced ET (Bounoua et al., 2010). Moreover, Skinner et al. (2017) found that the stomatal closure effect dominated the LAI effect in one model (CCSM4). It is therefore possible that the maximal approach used here for LAI changes may overestimate the importance of LAI compared to changes in conductance and other plant physiological effects in Earth system models with dynamic vegetation. Yet it also should be noted that there is substantial variation across models' stomatal conductance sensitivities to elevated CO<sub>2</sub> (De Kauwe et al., 2013; Y. Yang et al., 2019), making the extent to which this effect ameliorates dry climate conditions and other vegetation effects highly subject to model sensitivities.

The ability of ESMs to incorporate these vegetation responses has important implications for drought assessment. Previous work has shown that offline drought metrics based largely on atmospheric demand project widespread and strong future regional drying (Milly & Dunne, 2016; Swann, 2018; Y. Yang et al., 2019). These responses may be biased dry due to the exclusion of plant physiological processes in these calculations, namely stomatal closure under high CO<sub>2</sub> conditions (Milly & Dunne, 2016; Swann, 2018). ESMs therefore do have the advantage of explicitly including these plant processes and can thus more comprehensively assess, in a “plant-centric” way, the hydroclimate impacts under increasing CO<sub>2</sub>, despite structural limitations inherent to all models. Our simplified experiments show that while reduced conductance can attenuate regional soil moisture losses under high CO<sub>2</sub>, the sensitivity to LAI change may also be strong and can offset these responses leading to reduced regional water availability. As such, future drought assessments should strive to better incorporate the role of multiple, and importantly competing, plant responses to elevated CO<sub>2</sub>.

Of additional consideration are the timescales on which these effects and processes occur. Stomatal conductance responses to rising CO<sub>2</sub> occur more rapidly than the growth of vegetation structures and LAI, and thus LAI-induced cooling effects may lag initial vegetation biophysical warming (Andrews et al., 2011; Bounoua et al., 2010). For transient future climate simulations, additional evaluation is required to isolate “fast” (within a growing season) and “slow” (years to decades) vegetation responses (Andrews et al., 2011; Betts et al., 1997). More coordinated diagnostic analyses are also warranted to understand the disparate and combined influences of conductance and LAI on moisture recycling and atmospheric circulation under high CO<sub>2</sub>, specifically as they alter regional precipitation patterns that drive further vegetation feedbacks. Changes in circulation and subsequent precipitation patterns have been documented in a number of previous studies (Chadwick et al., 2019; Douville et al., 2000; Pu & Dickinson, 2014; Skinner et al., 2017), and more systematic analyses of the relative contributions of moisture convergence and localized recycling could add value to these efforts. A final important consideration is associated with the use of ESM experiments to represent “real world” vegetation growth and ecosystem responses that are often limited by many more factors than current models can incorporate or simulate reasonably. Such factors include, but are not limited to, nutrient limitation and cycling, the prevalence of pests and diseases (particularly alongside warming trends), extreme climate events, and the complex dynamics of mortality and ecological succession (Reich et al., 2014).

Lastly, our simulations do not consider the potential impacts of land use and land cover change (LULCC). It is important to note, however, that hydroclimate changes associated with vegetation interactions will also strongly depend on anthropogenic LULCC and that these effects will substantially differ regionally. For example, McDermid et al. (2019) show that intensive, industrialized cropping systems, such as those of the US Midwest and Great Plains, can alter seasonal and regional soil moisture availability and land-atmosphere coupling relative to natural vegetation, due in large part to their different LAI and annual growth cycles. In tropical areas experiencing rapid deforestation, there have also been slight declines in precipitation and ET and increases in surface temperature and runoff, although there are likely thresholds beyond which these effects are significantly amplified (Lawrence et al., 2015; Lejeune et al., 2015; Swann et al., 2015). Future work should aim to disentangle LULCC impacts from plant physiological responses, for example using the newest CMIP6 Shared Socio-economic Pathway scenarios and/or experiments run as part of the Landuse Model Intercomparison Project (D. M. Lawrence et al., 2016).

#### 4. Conclusions

Biophysical vegetation feedbacks under high CO<sub>2</sub> can have pronounced impacts on regional climate changes. To better understand these feedbacks, we have presented a series of idealized global climate model sensitivity experiments that focus on, and explicitly disentangle, two key vegetation effects: reduced stomatal conductance and enhanced leaf area. We have evaluated the influence of these effects both independently and assessed their linear and nonlinear interactions. Our results show substantial regional variation in the strength of these feedbacks, the interactions between these effects, and their resulting hydroclimate impacts.

Enhanced LAI exacerbates soil moisture deficits across water-limited domains, including the US Southwest, Iberian Peninsula, Middle East, eastern Australia, and central and eastern Asia. LAI effects also attenuate warming under higher CO<sub>2</sub> by ~0.5°C–1°C in the US Southwest, central Asia, and southeastern Asia. Conductance effects are strongest across mid-to high latitudes in the Northern Hemisphere, contributing ~1°C of regional warming during the growing season and reducing precipitation by ~10%–20%. In some regions, we find substantial nonlinear interactions between enhanced leaf areas and reduced conductance that produce either competing or mutually amplifying responses. Compared to the sum of effects, these nonlinearities reduce warming across Europe and northern China, likely due to enhanced canopy evaporation, which reduces the vapor pressure deficit, weakens the conductance response, and increases low-level cloud cover. In northeastern Australia, these nonlinear effects enhance regional drying by increasing atmospheric stability and further reducing summer precipitation by >10%. Additional experiments in which LAI changes are constrained by a CMIP6 multi-model ensemble under high CO<sub>2</sub> forcing produce hydroclimate responses generally similar to those of our 50% LAI increase sensitivity test in sign, magnitude, and geospatial distribution. Differences arise at lower latitudes, where our sensitivity test overestimates the LAI contribution compared to the CMIP6 ensemble, and at high latitudes where the greater CMIP6 LAI changes produce stronger climate responses.

Our results quantify the sensitivity of these simulated feedbacks in a modeled environment, particularly with respect to LAI gains under high CO<sub>2</sub>, and underscore the need for improved representation of biophysical processes in vegetation within simulations of future climate change. To enable continued model improvement, an emerging number of frameworks for model benchmarking and comparisons to observations are increasingly available (e.g., Medlyn et al., 2015). We suggest that such coordinated data and model efforts be a priority for the ecological and hydrological research communities and for applications in land and water management.

#### Acknowledgments

B.I. Cook, R. Seager, and A.P. Williams were all supported for this work by the NASA Modeling, Analysis, and Prediction program (NASA #80NSS-C17K0265). J.S. Mankin was supported by the NOAA Modeling, Analysis, Predictions and Projections program (NOAA MAPP NA20OAR4310414). M.D.K. acknowledge support from Australian Research Council (ARC) Centre of Excellence for Climate Extremes (CE170100023), the ARC Discovery Grants (DP190101823, DP180101253) and the NSW Research Attraction and Acceleration Program. Resources supporting this work were provided by the NASA High-End Computing (HEC) Program through the NASA Center for Climate Simulation (NCCS) at Goddard Space Flight Center. The GISS ModelE code used here resides within the ModelE development repository and is available upon request from the corresponding author. Resources supporting this work were provided by the NASA High-End Computing (HEC) Program through the NASA Center for Climate Simulation (NCCS) at Goddard Space Flight Center.

#### Conflict of Interest

All authors declare no conflicts of interests.

#### Data Availability Statement

Results here are based on ModelE tag modelE\_AR5\_v2\_branch, which is an intermediate version of the GISS ModelE2 and is not a publicly released version but is available in the developer repository. All the input files and simulation output used in this study are publicly available at: <https://doi.org/10.5281/zenodo.3662573>.

#### References

- Abramopoulos, F., Rosenzweig, C., & Choudhury, B. (1988). Improved ground hydrology calculations for Global Climate Models (GCMs): Soil water movement and evapotranspiration. *Journal of Climate*, 1, 921–941. [https://doi.org/10.1175/1520-0442\(1988\)001<0921:IGHCFG>2.0.CO;2](https://doi.org/10.1175/1520-0442(1988)001<0921:IGHCFG>2.0.CO;2)
- Ainsworth, E. A., & Rogers, A. (2007). The response of photosynthesis and stomatal conductance to rising [CO<sub>2</sub>]: Mechanisms and environmental interactions. *Plant, Cell and Environment*, 30, 258–270. <https://doi.org/10.1111/j.1365-3040.2007.01641.x>
- Andrews, T., Doutriaux-Boucher, M., Boucher, O., & Forster, P. M. (2011). A regional and global analysis of carbon dioxide physiological forcing and its impact on climate. *Climate Dynamics*, 36(3–4), 783–792. <https://doi.org/10.1007/s00382-010-0742-1>
- Armeth, A., Harrison, S. P., Zaehle, S., Tsigaridis, K., Menon, S., Bartlein, P. J., et al. (2010). Terrestrial biogeochemical feedbacks in the climate system. *Nature Geoscience*, 3(8), 525–532. <https://doi.org/10.1038/ngeo905>

- Ball, J. T., Woodrow, I. E., Berry, J. A., Ball, J., Timothy, W., I. E., & Berry, J. A. (1987). A model predicting stomatal conductance and its contribution to the control of photosynthesis under different environmental conditions. *Progress in Photosynthesis Research*, *IV*(953), 221–224. <https://doi.org/citeulike-article-id:8423355>
- Betts, R. A., Cox, P. M., Lee, S. E., & Woodward, F. I. (1997). Contrasting physiological and structural vegetation feedbacks in climate change simulations. *Nature*, *387*, 796–799. Retrieved from <https://ingrid.lidgo.columbia.edu/>
- Bounoua, L., Hall, F. G., Sellers, P. J., Kumar, A., Collatz, G. J., Tucker, C. J., & Imhoff, M. L. (2010). Quantifying the negative feedback of vegetation to greenhouse warming: A modeling approach. *Geophysical Research Letters*, *37*(23) n/a–n/a. <https://doi.org/10.1029/2010GL045338>
- Byrne, M. P., & O’Gorman, P. A. (2013). Link between land-ocean warming contrast and surface relative humidities in simulations with coupled climate models. *Geophysical Research Letters*, *40*(19), 5223–5227. <https://doi.org/10.1002/grl.50971>
- Canuto, V. M., & Dubovikov, M. S. (1996). A dynamical model for turbulence. I. General formalism. *Physics of Fluids*, *8*(2), 571–586. <https://doi.org/10.1063/1.868842>
- Chadwick, R., Ackerley, D., Ogura, T., & Dommenges, D. (2019). Separating the influences of land warming, the direct CO<sub>2</sub> effect, the plant physiological effect, and SST warming on regional precipitation changes. *Journal of Geophysical Research: Atmospheres*, *124*(2), 624–640. <https://doi.org/10.1029/2018JD029423>
- Chen, C., Park, T., Wang, X., Piao, S., Xu, B., Chaturvedi, R. K., et al. (2019). China and India lead in greening of the world through land-use management. *Nature Sustainability*, *2*(2), 122–129. <https://doi.org/10.1038/s41893-019-0220-7>
- Collatz, G. J., Ribas-Carbo, M., & Berry, J. A. (1992). Coupled photosynthesis-stomatal conductance model for leaves of C<sub>4</sub> plants. *Australian Journal of Plant Physiology*, *19*, 519–538.
- De Kauwe, M. G., Keenan, T. F., Medlyn, B. E., Colin Prentice, I., & Terrer, C. (2016). *Satellite based estimates underestimate the effect of CO<sub>2</sub> fertilization on net primary productivity*. Nature Publishing Group. <https://doi.org/10.1038/nclimate3105>
- De Kauwe, M. G., Medlyn, B. E., Zaehle, S., Walker, A. P., Dietze, M. C., Hickler, T., et al. (2013). Forest water use and water use efficiency at elevated CO<sub>2</sub>: A model-data intercomparison at two contrasting temperate forest FACE sites. *Global Change Biology*, *19*(6), 1759–1779. <https://doi.org/10.1111/gcb.12164>
- De Kauwe, M. G., Medlyn, B. E., Zaehle, S., Walker, A. P., Dietze, M. C., Wang, Y.-P., et al. (2014). Where does the carbon go? A model-data intercomparison of vegetation carbon allocation and turnover processes at two temperate forest free-air CO<sub>2</sub> enrichment sites. *New Phytologist*, *203*(3), 883–899. <https://doi.org/10.1111/nph.12847>
- Donohue, R. J., Roderick, M. L., McVicar, T. R., & Farquhar, G. D. (2013). Impact of CO<sub>2</sub> fertilization on maximum foliage cover across the globe’s warm, arid environments. *Geophysical Research Letters*, *40*(12), 3031–3035. <https://doi.org/10.1002/grl.50563>
- Douville, H., Planton, S., Royer, J.-F., Stephenson, D. B., Tyteca, S., Kergoat, L., et al. (2000). Importance of vegetation feedbacks in doubled-CO<sub>2</sub> climate experiments. *Journal of Geophysical Research*, *105*(D11), 14841–14861. <https://doi.org/10.1029/1999JD901086>
- Duursma, R. A., Gimeno, T. E., Boer, M. M., Crous, K. Y., Tjoelker, M. G., & Ellsworth, D. S. (2016). Canopy leaf area of a mature evergreen Eucalyptus woodland does not respond to elevated atmospheric [CO<sub>2</sub>] but tracks water availability. *Global Change Biology*, *22*(4), 1666–1676. <https://doi.org/10.1111/gcb.13151>
- Eamus, D., & Jarvis, P. G. (1989). The direct effects of increase in the global atmospheric CO<sub>2</sub> concentration on natural and commercial temperate trees and forests. *Advances in Ecological Research*, *19*(C), 1–55. [https://doi.org/10.1016/S0065-2504\(08\)60156-7](https://doi.org/10.1016/S0065-2504(08)60156-7)
- Eyring, V., Bony, S., Meehl, G. A., Senior, C., Stevens, B., Stouffer, R. J., & Taylor, K. E. (2015). Overview of the Coupled Model Intercomparison Project Phase 6 (CMIP6) experimental design and organisation. *Geoscientific Model Development Discussions*, *8*(12), 10539–10583. <https://doi.org/10.5194/gmdd-8-10539-2015>
- Farquhar, G. D., & von Caemmerer, S. (1982). Modelling of photosynthetic response to environmental conditions. In *Physiological plant ecology II* (pp. 549–587). Berlin: Springer Berlin Heidelberg. [https://doi.org/10.1007/978-3-642-68150-9\\_17](https://doi.org/10.1007/978-3-642-68150-9_17)
- Faticchi, S., Leuzinger, S., Paschalis, A., Langley, J. A., Donnellan Barraclough, A., & Hovenden, M. J. (2016). Partitioning direct and indirect effects reveals the response of water-limited ecosystems to elevated CO<sub>2</sub>. *Proceedings of the National Academy of Sciences of the United States of America*, *113*(45), 12757–12762. <https://doi.org/10.1073/pnas.1605036113>
- Forkel, M., Carvalhais, N., Röttenbeck, C., Keeling, R., Heimann, M., Thonicke, K., et al. (2016). Enhanced seasonal CO<sub>2</sub> exchange caused by amplified plant productivity in northern ecosystems. *Science (New York, NY)*, *351*(6274), 696–699. <https://doi.org/10.1126/science.aac4971>
- Forzieri, G., Alkama, R., Miralles, D. G., & Cescatti, A. (2017). Satellites reveal contrasting responses of regional climate to the widespread greening of Earth. *Science*, *356*, 1180–1184. <https://doi.org/10.1126/science.aal1727>
- Frank, D. C., Poulter, B., Saurer, M., Esper, J., Huntingford, C., Helle, G., et al. (2015). Water-use efficiency and transpiration across European forests during the Anthropocene. *Nature Climate Change*, *5*(6), 579–583. <https://doi.org/10.1038/nclimate2614>
- Friedl, M. A., Sulla-Menashe, D., Tan, B., Schneider, A., Ramankutty, N., Sibley, A., & Huang, X. (2010). MODIS Collection 5 global land cover: Algorithm refinements and characterization of new datasets. *Remote Sensing of Environment*, *114*, 168–182. <https://doi.org/10.1016/j.rse.2009.08.016>
- Friend, A. D., & Kiang, N. Y. (2005). Land surface model development for the GISS GCM: Effects of improved canopy physiology on simulated climate. *Journal of Climate*, *18*(15), 2883–2902. <https://doi.org/10.1175/JCLI3425.1>
- Halladay, K., & Good, P. (2017). Non-linear interactions between CO<sub>2</sub> radiative and physiological effects on Amazonian evapotranspiration in an Earth system model. *Climate Dynamics*, *49*(7–8), 2471–2490. <https://doi.org/10.1007/s00382-016-3449-0>
- Hansen, J., Russell, G., Rind, D., Stone, P., Lacis, a., Lebedeff, S., et al. (1983). Efficient three-dimensional global models for climate studies: Models I and II. *Monthly Weather Review*. [https://doi.org/10.1175/1520-0493\(1983\)111<0609:ETDGMF>2.0.CO;2](https://doi.org/10.1175/1520-0493(1983)111<0609:ETDGMF>2.0.CO;2)
- Harris, I., Jones, P. D., Osborn, T. J., & Lister, D. H. (2014). Updated high-resolution grids of monthly climatic observations – The CRU TS3.10 Dataset. *International Journal of Climatology*, *34*(3), 623–642. <https://doi.org/10.1002/joc.3711>
- Holtlag, A. A. M., & Boville, B. A. (1993). Local versus nonlocal boundary-layer diffusion in a global climate model. *Journal of Climate*, *6*(10), 1825–1842. [https://doi.org/10.1175/1520-0442\(1993\)006<1825:LVNBLD>2.0.CO;2](https://doi.org/10.1175/1520-0442(1993)006<1825:LVNBLD>2.0.CO;2)
- Holtlag, A. A. M., & Chin-Hoh, M. (1991). Eddy diffusivity and countergradient transport in the convective atmospheric boundary layer. *Journal of the Atmospheric Sciences*, *48*(14), 1690–1698. [https://doi.org/10.1175/1520-0469\(1991\)048<1690:EDACTI>2.0.CO;2](https://doi.org/10.1175/1520-0469(1991)048<1690:EDACTI>2.0.CO;2)
- Joshi, M. M., Gregory, J. M., Webb, M. J., Sexton, D. M. H., & Johns, T. C. (2008). Mechanisms for the land/sea warming contrast exhibited by simulations of climate change. *Climate Dynamics*, *30*(5), 455–465. <https://doi.org/10.1007/s00382-007-0306-1>
- Jung, M., Reichstein, M., Ciais, P., Seneviratne, S. I., Sheffield, J., Goulden, M. L., et al. (2010). Recent decline in the global land evapotranspiration trend due to limited moisture supply. *Nature*, *467*, 951–954. <https://doi.org/10.1038/nature09396>
- Kala, J., De Kauwe, M. G., Pitman, A. J., Lorenz, R., Medlyn, B. E., Wang, Y.-P., et al. (2015). Implementation of an optimal stomatal conductance scheme in the Australian Community Climate Earth Systems Simulator (ACCESS1.3b). *Geoscientific Model Development*, *8*(12), 3877–3889. <https://doi.org/10.5194/gmd-8-3877-2015>

- Kala, J., De Kauwe, M. G., Pitman, A. J., Medlyn, B. E., Wang, Y. P., Lorenz, R., & Perkins-Kirkpatrick, S. E. (2016). Impact of the representation of stomatal conductance on model projections of heatwave intensity. *Scientific Reports*, 6. <https://doi.org/10.1038/srep23418>
- Keenan, T. F., Hollinger, D. Y., Bohrer, G., Dragoni, D., Munger, J. W., Schmid, H. P., & Richardson, A. D. (2013). Increase in forest water-use efficiency as atmospheric carbon dioxide concentrations rise. *Nature*, 499(7458), 324–327. <https://doi.org/10.1038/nature12291>
- Kelley, M., Schmidt, G. A., Nazarenko, L. S., Bauer, S. E., Ruedy, R., Russell, G. L., et al. (2020). GISS-E2.1: Configurations and climatology. *Journal of Advances in Modeling Earth Systems*, 12(8). <https://doi.org/10.1029/2019MS002025>
- Kergoat, L., Lafont, S., Douville, H., Berthelot, B., Dedieu, G., Planton, S., & Royer, J. (2002). Impact of doubled CO<sub>2</sub> on global-scale leaf area index and evapotranspiration: Conflicting stomatal conductance and LAI responses. *Journal of Geophysical Research*, 107(D24), 4808. <https://doi.org/10.1029/2001JD001245>
- Kim, Y., Moorcroft, P. R. P., Aleinov, I., Puma, M. J., & Kiang, N. Y. (2015). Variability of phenology and fluxes of water and carbon with observed and simulated soil moisture in the Ent Terrestrial Biosphere Model (Ent TBM version 1.0.1.0.0). *Geoscientific Model Development*, 8(12), 3837–3865. <https://doi.org/10.5194/gmd-8-3837-2015>
- Kovenock, M., & Swann, A. L. S. (2018). Leaf trait acclimation amplifies simulated climate warming in response to elevated carbon dioxide. *Global Biogeochemical Cycles*, 32(10), 1437–1448. <https://doi.org/10.1029/2018GB005883>
- Lawrence, D., & VandeCar, K. (2015). Effects of tropical deforestation on climate and agriculture. *Nature Climate Change*, 5(1), 27–36. <https://doi.org/10.1038/nclimate2430>
- Lawrence, D. M., Hurtt, G. C., Arneth, A., Brovkin, V., Calvin, K. V., Jones, A. D., et al. (2016). The Land Use Model Intercomparison Project (LUMIP) contribution to CMIP6: rationale and experimental design. *Geoscientific Model Development*, 9, 2973–2998. <https://doi.org/10.5194/gmd-9-2973-2016>
- Leakey, A. D. B., Ainsworth, E. A., Bernacchi, C. J., Rogers, A., Long, S. P., & Ort, D. R. (2009). Elevated CO<sub>2</sub> effects on plant carbon, nitrogen, and water relations: Six important lessons from FACE. *Journal of Experimental Botany*, 60(10), 2859–2876. <https://doi.org/10.1093/jxb/erp096>
- Lejeune, Q., Davin, E. L., Guillod, B. P., & Seneviratne, S. I. (2015). Influence of Amazonian deforestation on the future evolution of regional surface fluxes, circulation, surface temperature and precipitation. *Climate Dynamics*, 44(9–10), 2769–2786. <https://doi.org/10.1007/s00382-014-2203-8>
- Lemordant, L., Gentine, P., Swann, A. S., Cook, B. I., & Scheff, J. (2018). Critical impact of vegetation physiology on the continental hydrologic cycle in response to increasing CO<sub>2</sub>. *Proceedings of the National Academy of Sciences of the United States of America*, 115(16), 4093–4098. <https://doi.org/10.1073/pnas.1720712115>
- Mahowald, N., Lo, F., Zheng, Y., Harrison, L., Funk, C., Lombardozi, D., & Goodale, C. (2016). Projections of leaf area index in earth system models. *Earth System Dynamics*, 7(1), 211–229. <https://doi.org/10.5194/esd-7-211-2016>
- Mankin, J. S., Seager, R., Smerdon, J. E., Cook, B. I., & Williams, A. P. (2019). Mid-latitude freshwater availability reduced by projected vegetation responses to climate change. *Nature Geoscience*. <https://doi.org/10.1038/s41561-019-0480-x>
- Mankin, J. S., Seager, R., Smerdon, J. E., Cook, B. I., Williams, A. P., & Horton, R. M. (2018). Blue water trade-offs with vegetation in a CO<sub>2</sub>-enriched climate. *Geophysical Research Letters*, 45(7), 3115–3125. <https://doi.org/10.1002/2018GL077051>
- Mankin, J. S., Smerdon, J. E., Cook, B. I., Williams, A. P., & Seager, R. (2017). The curious case of projected twenty-first-century drying but greening in the American West. *Journal of Climate*, 30, 8689–8710. <https://doi.org/10.1175/JCLI-D-17-0213.1>
- McDermid, S. S., Montes, C., Cook, B. I., Puma, M. J., Kiang, N. Y., & Aleinov, I. (2019). The sensitivity of land-atmosphere coupling to modern agriculture in the northern midlatitudes. *Journal of Climate*, 32(2). <https://doi.org/10.1175/JCLI-D-17-0799.1>
- Medlyn, B. E., Zaehle, S., De Kauwe, M. G., Walker, A. P., Dietze, M. C., Hanson, P. J., et al. (2015). Using ecosystem experiments to improve vegetation models. *Nature Climate Change*, 5(6), 528–534. <https://doi.org/10.1038/nclimate2621>
- Miller, R. L. (2014). CMIP5 historical simulations (1850–2012) with GISSModelE2 Ron. *Journal of Advances in Modeling Earth Systems*, 441–477. <https://doi.org/10.1002/2013MS000266>
- Milly, P. C. D., & Dunne, K. A. (2016). Potential evapotranspiration and continental drying. *Nature Climate Change*, 6(10), 946–949. <https://doi.org/10.1038/nclimate3046>
- Mooney, H. A., Drake, B. G., Luxmoore, R. J., Oechel, W. C., & Pitelka, L. F. (1991). Predicting ecosystem responses to elevated CO<sub>2</sub> concentrations. *BioScience*, 41(2), 96–104. <https://doi.org/10.2307/1311562>
- Morgan, J. A., Lecain, D. R., Pendall, E., Blumenthal, D. M., Kimball, B. A., Carrillo, Y., et al. (2011). C4 grasses prosper as carbon dioxide eliminates desiccation in warmed semi-arid grassland. *Nature*, 476, 202–205. <https://doi.org/10.1038/nature10274>
- Morison, J. I. L. (1985). Sensitivity of stomata and water use efficiency to high CO<sub>2</sub>. *Plant, Cell and Environment*, 8(6), 467–474. <https://doi.org/10.1111/j.1365-3040.1985.tb01682.x>
- Myneni, R. B., Keeling, C. D., Tucker, C. J., Asrar, G., & Nemani, R. R. (1997). Increased plant growth in the northern high latitudes from 1981 to 1991. *Nature*, 386(6626), 698–702. <https://doi.org/10.1038/386698a0>
- Ni-Meister, W., Yang, W., & Kiang, N. Y. (2010). A clumped-foliage canopy radiative transfer model for a global dynamic terrestrial ecosystem model. I: Theory. *Agricultural and Forest Meteorology*, 150(7–8), 881–894. <https://doi.org/10.1016/j.agrformet.2010.02.009>
- Norby, R. J., DeLucia, E. H., Gielen, B., Calfapietra, C., Giardina, C. P., Kings, J. S., et al. (2005). Forest response to elevated CO<sub>2</sub> is conserved across a broad range of productivity. *Proceedings of the National Academy of Sciences of the United States of America*, 102(50), 18052–18056. <https://doi.org/10.1073/pnas.0509478102>
- Norby, R. J., & Zak, D. R. (2011). Ecological lessons from free-air CO<sub>2</sub> enrichment (FACE) experiments. *Annual Review of Ecology, Evolution and Systematics*, 42, 181–203. <https://doi.org/10.1146/annurev-ecolsys-102209-144647>
- Poorter, H., Niinemets, Ü., Ntagkas, N., Siebenkäs, A., Mäenpää, M., Matsubara, S., & Pons, T. L. (2019). A meta-analysis of plant responses to light intensity for 70 traits ranging from molecules to whole plant performance. In *New phytologist*. Blackwell Publishing Ltd. <https://doi.org/10.1111/nph.15754>
- Pu, B., & Dickinson, R. E. (2014). Hydrological changes in the climate system from leaf responses to increasing CO<sub>2</sub>. *Climate Dynamics*, 42(7–8), 1905–1923. <https://doi.org/10.1007/s00382-013-1781-1>
- Reich, P. B., Hobbie, S. E., & Lee, T. D. (2014). Plant growth enhancement by elevated CO<sub>2</sub> eliminated by joint water and nitrogen limitation. *Nature Geoscience*, 7(12), 920–924. <https://doi.org/10.1038/ngeo2284>
- Reich, P. B., Hobbie, S. E., Lee, T. D., & Pastore, M. A. (2018). Unexpected reversal of C3 versus C4 grass response to elevated CO<sub>2</sub> during a 20-year field experiment. *Science*, 360(6386), 317–320. <https://doi.org/10.1126/science.aas9313>
- Rosenzweig, C., & Abramopoulos, F. (1997). Land-surface model development for the GISS GCM. *Journal of Climate*, 10(8), 2040–2054. [https://doi.org/10.1175/1520-0442\(1997\)010<2040:LSMDFT>2.0.CO;2](https://doi.org/10.1175/1520-0442(1997)010<2040:LSMDFT>2.0.CO;2)
- Saint-Lu, M., Chadwick, R., Lambert, F. H., & Collins, M. (2019). Surface warming and atmospheric circulation dominate rainfall changes over tropical rainforests under global warming. *Geophysical Research Letters*, 46(22), 13410–13419. <https://doi.org/10.1029/2019GL085295>

- Schmidt, G. A., Kelley, M., Nazarenko, L., Ruedy, R., Russell, G. L., Aleinov, I., et al. (2014). Configuration and assessment of the GISS ModelE2 contributions to the CMIP5 archive. *Journal of Advances in Modeling Earth Systems*, 6, 141–184. <https://doi.org/10.1002/2013MS000265>
- Schmidt, G. A., Ruedy, R., Hansen, J. E., Aleinov, I., Bell, N., Bauer, M., et al. (2006). Present-day atmospheric simulations using GISS ModelE: Comparison to in situ, satellite, and reanalysis data. *Journal of Climate*, 19(1), 153–192. <https://doi.org/10.1175/JCLI3612.1>
- Schneider, U., Becker, A., Finger, P., Meyer-Christoffer, A., Ziese, M., & Rudolf, B. (2014). GPCC's new land surface precipitation climatology based on quality-controlled in situ data and its role in quantifying the global water cycle. *Theoretical and Applied Climatology*, 115(1–2), 15–40. <https://doi.org/10.1007/s00704-013-0860-x>
- Sellers, P. J., Bounoua, L., Collatz, G. J., Randall, D. A., Dazlich, D. A., Los, S. O., et al. (1996). Comparison of radiative and physiological effects of doubled atmospheric CO<sub>2</sub> on climate. *Science*, 271(5254), 1402–1406. <https://doi.org/10.1126/science.271.5254.1402>
- Simard, M., Pinto, N., Fisher, J. B., & Baccini, A. (2011). Mapping forest canopy height globally with spaceborne lidar. *Journal of Geophysical Research: Biogeosciences*, 116(4), 1–12. <https://doi.org/10.1029/2011JG001708>
- Skinner, C. B., Poulsen, C. J., Chadwick, R., Diffenbaugh, N. S., & Fiorella, R. P. (2017). The role of plant CO<sub>2</sub> physiological forcing in shaping future daily-scale precipitation. *Journal of Climate*, 30(7), 2319–2340. <https://doi.org/10.1175/JCLI-D-16-0603.1>
- Skinner, C. B., Poulsen, C. J., & Mankin, J. S. (2018). Amplification of heat extremes by plant CO<sub>2</sub> physiological forcing. *Nature Communications*, 9(1), 1094. <https://doi.org/10.1038/s41467-018-03472-w>
- Smith, K., Reed, S. C., Cleveland, C., Ballantyne, A., Anderegg, W., Wieder, W., et al. (2015). Large divergence of satellite and Earth system model estimates of global terrestrial CO<sub>2</sub> fertilization. *Nature Climate Change*, 6, 1–11. <https://doi.org/10.1038/nclimate2879>
- Swann, A. L. S. (2018). Plants and drought in a changing climate. *Current Climate Change Reports*, 4(2), 192–201. <https://doi.org/10.1007/s40641-018-0097-y>
- Swann, A. L. S., Hoffman, F. M., Koven, C. D., & Randerson, J. T. (2016). Plant responses to increasing CO<sub>2</sub> reduce estimates of climate impacts on drought severity. *Proceedings of the National Academy of Sciences*, 113(36). <https://doi.org/10.1073/pnas.1604581113>
- Swann, A. L. S., Longo, M., Knox, R. G., Lee, E., & Moorcroft, P. R. (2015). Future deforestation in the Amazon and consequences for South American climate. *Agricultural and Forest Meteorology*, 214–215, 12–24. <https://doi.org/10.1016/j.agrformet.2015.07.006>
- Taylor, C. M., Jeu, D., Richard, A. M., Guichard, F., Harris, P. P., & Dorigo, W. a. (2012). In Afternoon rain more likely over drier soils (Vols. 9–12). <https://doi.org/10.1038/nature11377>
- Taylor, K. E., Stouffer, R. J., & Meehl, G. a. (2012). An overview of CMIP5 and the experiment design. *Bulletin of the American Meteorological Society*, 93(4), 485–498. <https://doi.org/10.1175/BAMS-D-11-00094.1>
- Tian, Y., Woodcock, C. E., Wang, Y., Privette, J. L., Shabanov, N. V., Zhou, L., et al. (2002a). Multiscale analysis and validation of the MODIS LAI product: I. Uncertainty assessment. *Remote Sensing of Environment*, 83(3), 414–430. [https://doi.org/10.1016/S0034-4257\(02\)00047-0](https://doi.org/10.1016/S0034-4257(02)00047-0)
- Tian, Y., Woodcock, C. E., Wang, Y., Privette, J. L., Shabanov, N. V., Zhou, L., et al. (2002b). Multiscale analysis and validation of the MODIS LAI product II. Sampling strategy. *Remote Sensing of Environment*, 83, 431–441. Retrieved from <https://cliveg.bu.edu/download/manuscripts/ytian04.pdf>
- Trancoso, R., Larsen, J. R., McVicar, T. R., Phinn, S. R., & McAlpine, C. A. (2017). CO<sub>2</sub>-vegetation feedbacks and other climate changes implicated in reducing base flow. *Geophysical Research Letters*, 44(5), 2310–2318. <https://doi.org/10.1002/2017GL072759>
- Ukkola, A. M., Prentice, I. C., Keenan, T. F., van Dijk, A. I. J. M., Viney, N. R., Myneni, R. B., & Bi, J. (2016). Reduced streamflow in water-stressed climates consistent with CO<sub>2</sub> effects on vegetation. *Nature Climate Change*, 6(1), 75–78. <https://doi.org/10.1038/nclimate2831>
- Van Der Sleen, P., Groenendijk, P., Vlam, M., Anten, N. P. R., Boom, A., Bongers, F., et al. (2015). No growth stimulation of tropical trees by 150 years of CO<sub>2</sub> fertilization but water-use efficiency increased. *Nature Geoscience*, 8(1), 24–28. <https://doi.org/10.1038/ngeo2313>
- Walker, A. P., De Kauwe, M. G., Bastos, A., Belmecheri, S., Georgiou, K., Keeling, R., et al. (2020). Integrating the evidence for a terrestrial carbon sink caused by increasing atmospheric CO<sub>2</sub>. In *New Phytologist*. <https://doi.org/10.1111/nph.16866>
- Warren, J. M., Pötzelsberger, E., Wullschlegel, S. D., Thornton, P. E., Hasenauer, H., & Norby, R. J. (2011). Ecohydrologic impact of reduced stomatal conductance in forests exposed to elevated CO<sub>2</sub>. *Ecohydrology*, 4(2), 196–210. <https://doi.org/10.1002/eco.173>
- Wieder, W. R., Cleveland, C. C., Lawrence, D. M., & Bonan, G. B. (2015). Effects of model structural uncertainty on carbon cycle projections: biological nitrogen fixation as a case study. *Environmental Research Letters*, 10(4), 044016. <https://doi.org/10.1088/1748-9326/10/4/044016>
- Yang, J., Medlyn, B. E., De Kauwe, M. G., & Duursma, R. A. (2018). Applying the concept of ecohydrological equilibrium to predict steady state leaf area index. *Journal of Advances in Modeling Earth Systems*, 10(8), 1740–1758. <https://doi.org/10.1029/2017MS001169>
- Yang, W., Ni-Meister, W., Kiang, N. Y., Moorcroft, P. R., Strahler, A. H., & Oliphant, A. (2010). A clumped-foliage canopy radiative transfer model for a Global Dynamic Terrestrial Ecosystem Model II: Comparison to measurements. *Agricultural and Forest Meteorology*, 150(7–8), 895–907. <https://doi.org/10.1016/j.agrformet.2010.02.008>
- Yang, W., Tan, B., Huang, D., Rautiainen, M., Shabanov, N. V., Wang, Y., et al. (2006). MODIS leaf area index products: From validation to algorithm improvement. *IEEE Transactions on Geoscience and Remote Sensing*, 44(7), 1885–1898. <https://doi.org/10.1109/TGRS.2006.871215>
- Yang, Y., Roderick, M. L., Zhang, S., McVicar, T. R., & Donohue, R. J. (2019). Hydrologic implications of vegetation response to elevated CO<sub>2</sub> in climate projections. In *Nature Climate Change*. Nature Publishing Group. <https://doi.org/10.1038/s41558-018-0361-0>
- Zaehle, S., Medlyn, B. E., De Kauwe, M. G., Walker, A. P., Dietze, M. C., Hickler, T., et al. (2014). Evaluation of 11 terrestrial carbon-nitrogen cycle models against observations from two temperate free-air CO<sub>2</sub> enrichment studies. *New Phytologist*, 202(3), 803–822. <https://doi.org/10.1111/nph.12697>
- Zeng, Z., Piao, S., Li, L. Z. X., Zhou, L., Ciais, P., Wang, T., et al. (2017). Climate mitigation from vegetation biophysical feedbacks during the past three decades. *Nature Climate Change*, 7, 432–436. <https://doi.org/10.1038/NCLIMATE3299>
- Zhang, K., Kimball, J. S., Nemani, R. R., Running, S. W., Hong, Y., Gourley, J. J., & Yu, Z. (2015). Vegetation greening and climate change promote multidecadal rises of global land evapotranspiration. *Scientific Reports*, 5(1), 15956. <https://doi.org/10.1038/srep15956>
- Zhu, Z., Piao, S., Myneni, R. B., Huang, M., Zeng, Z., Canadell, J. G., et al. (2016). Greening of the Earth and its drivers. *Nature Climate Change*, 6, 791–795. <https://doi.org/10.1038/NCLIMATE3004>
- Zwiers, F. W., von Storch, H., Zwiers, F. W., & Storch, H. von (1995). Taking serial correlation into account in tests of the mean. *Journal of Climate*, 8(2), 336–351. [https://doi.org/10.1175/1520-0442\(1995\)008<0336:TSCIAI>2.0.CO;2](https://doi.org/10.1175/1520-0442(1995)008<0336:TSCIAI>2.0.CO;2)